In situ generation of Ag nanoparticles during photopolymerization by using newly developed dyes-based three-component photoinitiating systems and the related 3D printing applications and their shape change behavior

Hong Chen, Guillaume Noirbent, Shaohui Liu, Yijun Zhang, Ke Sun, Fabrice Morlet-savary, Didier Gigmes, Pu Xiao, Frédéric Dumur, Jacques Lalevée

In situ generation of Ag nanoparticles during photopolymerization by using newly developed dyes-based three-component photoinitiating systems and the related 3D printing applications and their shape change behavior

Hong Chen[1,2] Guillaume Noirbent[3] Shaohui Liu[1,2] Yijun Zhang[1,2] Ke Sun[1,2] Fabrice Morlet-Savary[1,2] Didier Gigmes[3] Pu Xiao[4] Frédéric Dumur[3] Jacques Lalevée[1,2]

[1] Université de Haute-Alsace, CNRS, IS2M UMR 7361, F-68100 Mulhouse, France; jacques.lalevee@uha.fr
[2] Université de Strasbourg, France
[3] Aix Marseille Univ, CNRS, ICR UMR 7273, F-13397 Marseille, France ; frederic.dumur@univ-amu.fr

[4] Research School of Chemistry, Australian National University, Camberra, ACT 2601, Australia; pu.xiao@anu.edu.au

* Corresponding author: jacques.lalevee@uha.fr (J. L.), frederic.dumur@univ-amu.fr (F.D.); pu.xiao@anu.edu.au (P. X.).

Abstract: In this work, 12 different dyes centered on 2,5-diethylene-cyclopentane-1-one were firstly synthesized and used as high-performance photoinitiating systems (PISs) in combination with *bis*(4-*tert*-butylphenyl (Iod) and *bis*(4-*tert*-butylphenyl (amine) to induce the free radical photopolymerization (FRP) of the polyethylene glycol diacrylate (PEG-DA) and cationic photopolymerization (CP) of 3,4-epoxycyclohexylmethy l-3,4-epoxycyclohexanecarboxylate (EPOX) under a light-emitting diode (LED) at 405 nm. To demonstrate the involved reaction mechanisms, several characterization techniques were used, including steady state photolysis, emission spectroscopy, ESR-spin trapping experiments as well as cyclic voltammetry. In addition, excellent photopolymerization efficiency were followed by real-time FTIR spectroscopy. More interestingly, 3D patterns were successfully fabricated through the direct laser write (DLW) technology, which exhibits reversible swelling performance and reversible shape-memory effects caused by swelling and dehydration for the access to 4D printing.

Keywords: silver nanoparticles; reversible shape-memory effect; photopolymerization; 3D/4D printing; thermos-responsive and water-responsive.

1. Introduction

In recent years, due to the adjustable optical properties of metal nanoparticles (MNP) such as silver, gold or platinum, the potential applications of them in advanced materials like photovoltaic technology [1], electronic [2,3] and optical detection systems [4], solar concentrators/reflectors or filters [5-6]. etc, have attached great attention. In order to adapt to these new applications, a large amount of research on the synthesis and processing of metal nanoparticles has been carried out, whose purpose is to generate nano- or micro-layers on various substrates [7-8]. An appropriate synthesis method is the key to control the morphology and the size of MNP and its subsequent physical and optical properties. Many MNP synthesis routes e.g. chemical methods, radiation methods, solvothermal methods, etc, have been reported, which mainly relies on the precipitation of nanoparticles from the precursor solution by reducers [9-12]. However, most of them existence some disadvantages, for examples, require sophisticated fabrication equipment, induce expensive cost or lack of mechanical strength, et [13].

In order to avoid these drawbacks, composite materials based on nanoparticles and polymer matrix have recently attracted attention due to their synergistic effects [14-16]. Photopolymerization technology can provide a useful method for generating polymers suitable for various applications ranging from imaging, radiation curing, and optics technologies to (bio)medicine, microelectronics, and materials science, as its mild reaction conditions and controllability in time and space [17-19]. An excellent photoinitiator (PI) plays a vital role in the photopolymerization process, which induces the liquid monomers rapidly conversed into highly crosslinked solid polymers by absorbing the appropriate wavelengths of light to generate reactive species (e.g. cations, free radicals, anions…), furthermore, the reactive species can also reduce the metal salt to metal nanoparticles [20].

According to the abovementioned requirements, 12 new dyes centered on 2,5-diethylene-cyclopentane-1-one were firstly designed and synthesized, which combined with amines and Iod as photoinitiation system (PIS) to study their

polymerization efficiency for free radical polymerization (FRP) and cationic polymerization (CP). Subsequently, the photochemical mechanism involved in the polymerization process was studied in detail through steady-state photolysis, fluorescence quenching, cyclic voltammetry and electron spin resonance (ESR) experiments, and the calculation of free energy changes. Finally, the newly proposed photo-initiated system was used to successfully prepare a three-dimensional 3D pattern with a certain spatial resolution. This work proposes an efficient and environmentally friendly method that the photopolymerization process of the PEG-DA and the in-situ reduction of silver nitrate to AgNPs are concurrent carried out to obtain a PEG-polymer with a complete distribution of silver nanoparticles, which not only has reversibility swelling properties but also exhibits reversibility shape-memory effect. This innovative method is full of promise for the preparation of metal polymer coatings and the preparation of flexible conductive materials.

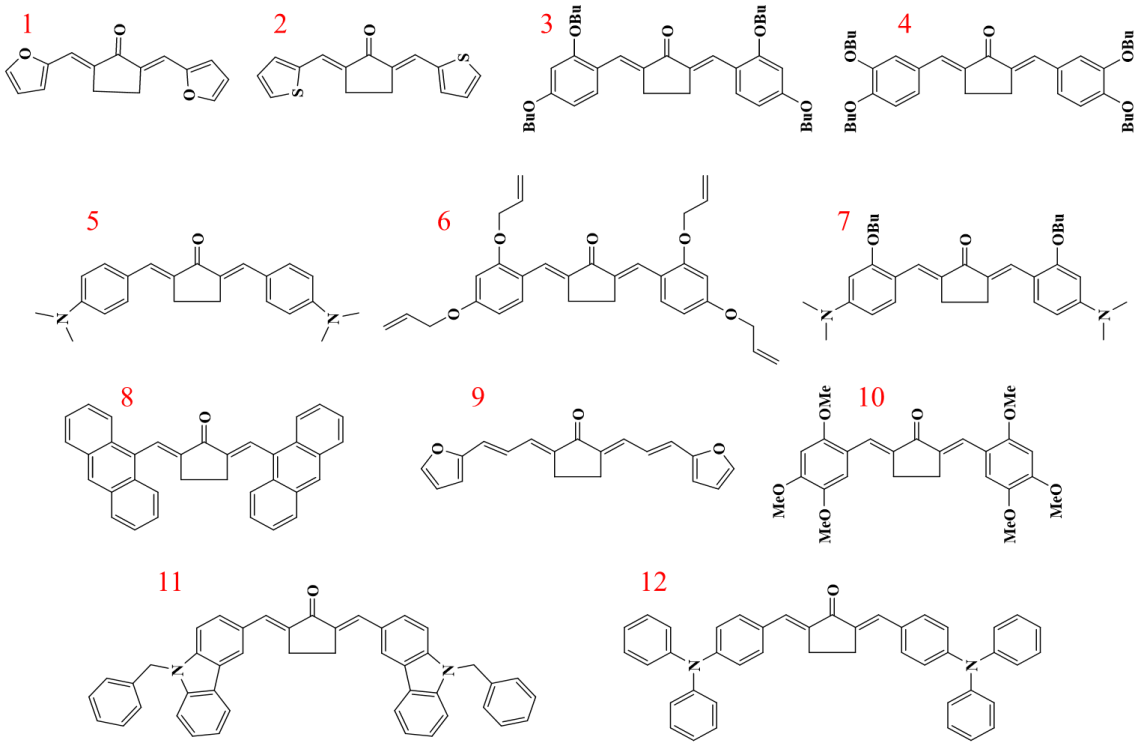

Scheme 1. Chemical structures of dyes 1-12.

2. Materials and Methods

2.1 Material

The 12 different chalcone-based dyes (1-12) were used as photoinitiators that prepared as reported in the SI, their molecular structures are given in the Scheme 1. The free radical photopolymerization monomer polyethylene glycol diacrylate (PEG-DA) was obtained from Sartomer-Europe, while the cationic photopolymerization benchmark monomer 3,4-epoxycyclohexylmethyl 3,4-epoxycyclohexanecarboxylate (EPOX) was purchased from Allnex. *Bis*-(4-*tert*-butylphenyl) iodonium hexafluorophosphate (Iod) used as co-initiator and ethyl 4-dimethylaminobenzoate (amine, EDB) used as electron donor were all purchased from Lambson Ltd. The electron capture agent Phenyl-*N*-*tert*-butylnitrone (PBN) was purchased from Sigma-Aldrich (St. Louis, MO, USA). Their corresponding chemical structures are presented in Scheme 2. The solvent (e.g., acetonitrile, dimethyl sulfoxide and *tert*-butylbenzene) uesed in this study were all of analytical grade and purchased from Sigma-Aldrich (St. Louis, MO, USA).

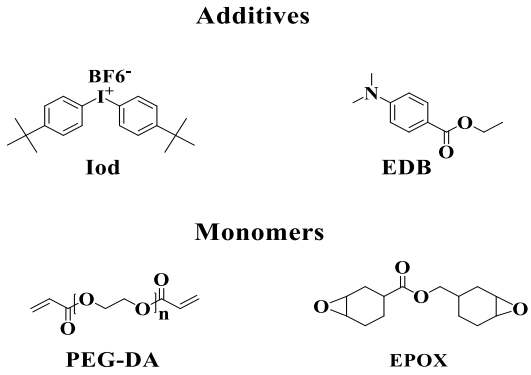

Scheme 2. The chemical structure of other additives and monomers used in this study.

2.2 Free Radical Photopolymerization (FRP) and Cationic Photopolymerizations (CP) Initiated by dye/Iod/amine PIS

Dyes/Iod/amine combinations were used as PIS for FRP and CP under near UV or visible light of LED 405nm (I_0 = 110 mW/cm^2) and 470nm (I_0 = mW/cm^2). The weight contents of each components were calculated from the weight of monomers (PEG-DA or EPOX), which are maintained at 0.1wt%/1.5wt%/1.5wt% (w/w/w), respectively. All these dyes were dispersed well in the resins (PEG-DA and EPOX). FRP of the PEG-DA (thickness about 20 μm or 2mm) was performed in laminated

condition to reduce the O_2 inhibition, while CP of EPOX (thickness ~20 μm) was carried out in air. The conversions of epoxy or acrylate functions were continuously monitored by real-time FTIR spectroscopy (JASCO FTIR 4100) which followed by the characteristic peaks around 790 cm^{-1} or 3700 cm^{-1} (EPOX) and 1600 cm^{-1} or 6160 cm^{-1} (PEG-DA), respectively [21].

2.3 UV-*Vis* Absorption Properties, Photolysis and Fluorescence Experiments of the Dyes.

The UV-*vis* absorption properties of the 12 different chalcones-based dyes and the photolysis of dyes based one-, two- and three- compound PIS (dyes, dyes/Iod, dyes/amine, dyes/Iod/amine) were studied by the JASCO V730 spectrophotometer. All of the dyes were dissolved in acetonitrile and analyzed with a concentration of 1×10^{-5} M for dyes and 0.01 M for Iod and EDB during the photolysis process. Moreover, their fluorescence properties were studied through the JASCO FP-6200 spectrofluorimeter in acetonitrile at the concentration about 1×10^{-5} M [22].

2.4 Redox Potentials of Dyes.

The redox potentials (E_{ox} and E_{red}) of chalcone-based dyes were determined by cyclic voltammetry that using tetrabutylammonium hexafluorophosphate as the supporting electrolyte in acetonitrile. Free energy change (ΔG^{S1}_{Iod} or ΔG^{S1}_{EDB}) for the electron transfer reaction between dyes with Iod/amine were calculated from equation 1 or 2, where E_{ox}, E_{red} and E^* are the oxidation potential of the electron donor, the reduction potential of the electron acceptor and the excited state energy level (calculated from the crossing point of UV-visible and fluorescence spectra), respectively. According to literature data, the reduction potential of Iod was -0.7 eV and the oxidation potential of EDB was 1.0 eV [23-24].

$$\Delta G^{S1}_{Iod} = E_{ox} - (-0.7) - E^* \quad (1)$$

$$\Delta G^{S1}_{EDB} = 1.0 - E_{red} - E^* \quad (2)$$

2.5 Electron Spin Resonance (ESR) Spin Trapping (ESR-ST) Experiments

An X-band spectrometer (Bruker EMX-plus) was used for ESR-ST experiments. The generated radicals were trapped by PBN at room temperature in N_2 saturated *tert*-butylbenzene solutions upon LED@405nm irradiation light. ESR spectrum simulated through WINSIM software [25].

2.6 Preparation of Silver nanoparticles (AgNPs) in DMF

Silver nanoparticles were prepared in DMF solution in the air. 0.4wt%-Dye/Iod/amine-based PIS (0.1wt%/1.5wt%1.5wt%) and 4wt%-$AgNO_3$ were dissolved in 10 mL DMF, after that sonicate the solution for 10 minutes and irradiated using LED@405nm (I_0 = 110 mW/cm^2) to prepare the AgNPs [26].

2.7 Preparation of AgNPs within PEG-polymers through in-situ Photopolymerization Process

Dye/Iod/amine (0.1wt%/1.5wt%1.5wt%) and $AgNO_3$ (4wt%) were dissolved in PEG-DA. The formulation is mixed with an ultrasonicator for 5 min to make the metal salt well distributed before polymerization. After that, the photopolymerization profile was followed by the real-time FTIR spectroscopy and the PEG-AgNPs nanocomposite film was obtained by coating the formulation on the glass plate using Bar Coaters and curing under LED@405nm.

2.8 TEM Experiments.

The morphology of the generated AgNPs within the DMF solvent and PEG-polymers were observed by a transmission electron microscope (TEM, FEI Quanta 250 FEG).

2.9 Laster Write Experiments

Laster write experiments were carried out using computer programmed laser diode at 405nm (Thorlabs, spot size is about 50 μm). Photosensitive formulations containing PEG-DA, dyes-based PIS and/without metal salt under solvent-free

conditions were written in the air and the obtained 3D patterns were analyzed using a numerical optical microscope (DSX-HRSU from Olympus Corporation) [27].

2.10 Swelling Experiment of PEG-polymers

The swelling experiments of PEG-polymers containing/without AgNPs were investigated by immersing in deionized water at room temperature. Then, the polymers (n = 3) were taken out to measure the wet weigh (W_t) after reaching the swelling equilibrium and compared with their initial wet weight (W_0), after that the swollen polymers were put in a 50 ^oC oven to remove the absorbed water. The swelling ratio (*Sr*) was defined according to equation 3, and the volume changes ratio of the patterns during the swelling process, namely the initial volume (V_1), the volume at swelling equilibrium (V_2) and the volume after dehydration (V_3), were calculated according to equation 4 [28, 29].

$$\boldsymbol{Sr\ (wt\%) = (Wt\text{-}Wo) / Wo \times 100} \quad \textbf{3)}$$

$$\boldsymbol{R\ (wt\%) = (V_2 / V_1) \times 100} \quad \textbf{4)}$$

2.11 Shape-Memory Effect of PEG-polymers containing/without AgNPs (4D behavior)

The reversible temporarily deformation effect of the polymerization products containing/without AgNPs were conducted *via* swelling and dehydration induced actuation: at first, the products were immersed into water for 1 min at room temperature; after that, took them out from water and put into oven around 80 °C for 20 min to dehydrate the swollen water; finally, the products were taken out into room temperature to recovery their original shapes.

3. Results and Discussion

The photo-physicochemical properties as well as the chemical mechanisms of 12 different proposed dyes as the photoinitiators have been investigated in details.

3.1. UV-*vis* Absorption Properties of the Chalcone-based Dyes in Acetonitrile

The absorption spectra of 12 different proposed dyes in acetonitrile were depicted Figure S1, while their absorption maxima (λ_{max}) as well as extinction coefficients (ε_{max}) at λ_{max} and at the emission wavelength of the LED@405 nm and LED@470 nm are summarized in the Table 1. In fact, all dyes exhibited a stronger absorption peaks at visible resign (λ > 390nm), while a weaker absorption peak or shoulder were observed at UV resign (λ < 300nm) for dyes 3, 5, 7, 8, 9, 10, 11 and 12. Furthermore, since the stronger maximum absorption peak of dye 5, 7 and 12 are appeared in the range from 460 nm to 480nm, while the other PIs were appeared in the range from 390 nm to 430nm, LED@405 nm and LED@470 nm have been chosen as the light source in this work to ensure a good overlap with the emission spectrum. Except the dye 8 whose extinction coefficients are all less than $5*10^3$ $M^{-1}cm^{-1}$, the other dyes exhibited higher extinction coefficients (ε_{max}) in the visible resign (e.g., 58 500 $M^{-1}cm^{-1}$, 13 620 $M^{-1}cm^{-1}$and 52 680 $M^{-1}cm^{-1}$ for dye 7 at λ_{max}, $\lambda_{@405nm}$ and $\lambda_{@470nm}$, respectively) corresponding to π-π* electronic transitions. In addition, the different substituents attached to the central part of 2,5-dimethylenecyclopentan-1-one will greatly affected their UV-*vis* absorption spectrum. Remarkably, the introduction of electron-donating groups causes a red-shift in the absorption spectrum, therefore the electron donating functions of these substituents are arranged as the following order: dye 7 >dye 5 and 12 > dye 9 and 10 > dye 11 and 8 > dye3, 4 and 6 > dye 1 and 2.

Chalcone-based dyes	λ_{max} **(nm)**	ε_{max} **($M^{-1}cm^{-1}$)**	$\varepsilon_{@405nm}$ **($M^{-1}cm^{-1}$)**	$\varepsilon_{@470nm}$ **($M^{-1}cm^{-1}$)**
1	396	41 980	37 050	270
2	392	40 840	33 590	110
3	400 274	41 770 69 250	41 610	2720
4	399	42 500	41 580	1280
5	460 274	57 400 37 300	23 700	53 446

6	397	38 150	36 700	1710
7	485 278	65 670 22 680	16 200	59 370
8	418 268	6970 12 890	6800	1600
9	428 283	61 130 15 340	50 310	16 540
10	427 280	42 062 14 160	32 270	14 380
11	421 236	36 350 46 810	30 560	10 160
12	460 298	47 620 35 060	25 300	44 400

Table 1. Light absorption properties of dyes 1-12 in acetonitrile: maximum absorption wavelengths λ_{max}; extinction coefficients at λ_{max} (ε_{max}) and extinction coefficients at the emission wavelength of the LED@405 nm ($\varepsilon_{@405nm}$) and LED@470 nm ($\varepsilon_{@470nm}$).

3.2 Photopolymerization Kinetics of the Proposed Dyes-based PISs.

3.2.1. Free radical polymerization (FRP) kinetics of PEG-DA.

The photoinitiation abilities of dye/Iod/amine (0.1wt%/1.5wt%/1.5wt%) based three-compound PISs for the FRP of PEG-DA were studied upon irradiation with LED@405nm or LED@470nm at room temperature. The different polymerization profiles can be found in Figure 1, and the final acrylate function conversions (FC) are simplified in Table 2. It can be seen that all these dyes-based PIS exhibited better photoinitiating efficiencies than the blank PIS (FC 76wt%) consisting of the co-initiator (Iod, 1.5wt%, w/w) and the electron donor (amine, 1.5wt%, w/w) upon irradiation with LED@405nm at the thickness about 20μm (Figure 1A). It demonstrated that the presence of the dyes is crucial to boost their polymerization performance. Remarkably, dyes 2, 3, 8 and 9-based PIS achieved more than 90wt% conversions within 50 s, which were much higher and faster than that obtained by other dyes-based PIS. However, under the same conditions, for the thick sample whose thickness is about 2mm, it's clearly that only dye 5-based PIS showed better photopolymerization kinetics in the comparision with the blank PIS (conversion: 92% of dye 5*vs* 87% of blank), while the conversion of other dyes-based PIS achieved are all less than 70% within 200s.

More interestingly, upon irradiation with the LED@470nm, the blank control that initiated by the Iod/amine-based PIS can't deep curing both at the thickness of 20μm and 2mm, while better photopolymerization kinetics were observed for the dyes-based PIS. Furthermore, as shown in Figure 1C, for the thin samples, the conversions of all dyes-based PIS achieved are all less than 90% which are smaller than that achieved under LED@405nm; while for the thick samples, dye 5-based PIS also achieved the best effectiveness (see Figure 1D) which can be assigned to its high molar extinction coefficients (e.g., 63 170 $M^{-1}cm^{-1}$, 27 360 $M^{-1}cm^{-1}$ and 58 880 $M^{-1}cm^{-1}$ for dye 5 at λ_{max}, $\lambda_{@405nm}$ and $\lambda_{@470nm}$ respectively, see table 1).

In comparison with the initiating ability including the final monomer conversions (Table 2) and the rates of polymerization (the initial slope of the curves, Figure 1) of all dyes-based PIS, LED@405nm is more suitable as the light source to initiate the FRP of PEG-DA than the LED@470nm. Under this condition, dyes 2, 3, 5, 8 and 9 were selected and proved to be excellent candidates to boost the polymerization for PEG-DA with the thickness of 20 μm or 2 mm in laminate, matching with their higher extinction coefficient at the wavelength of 405nm.

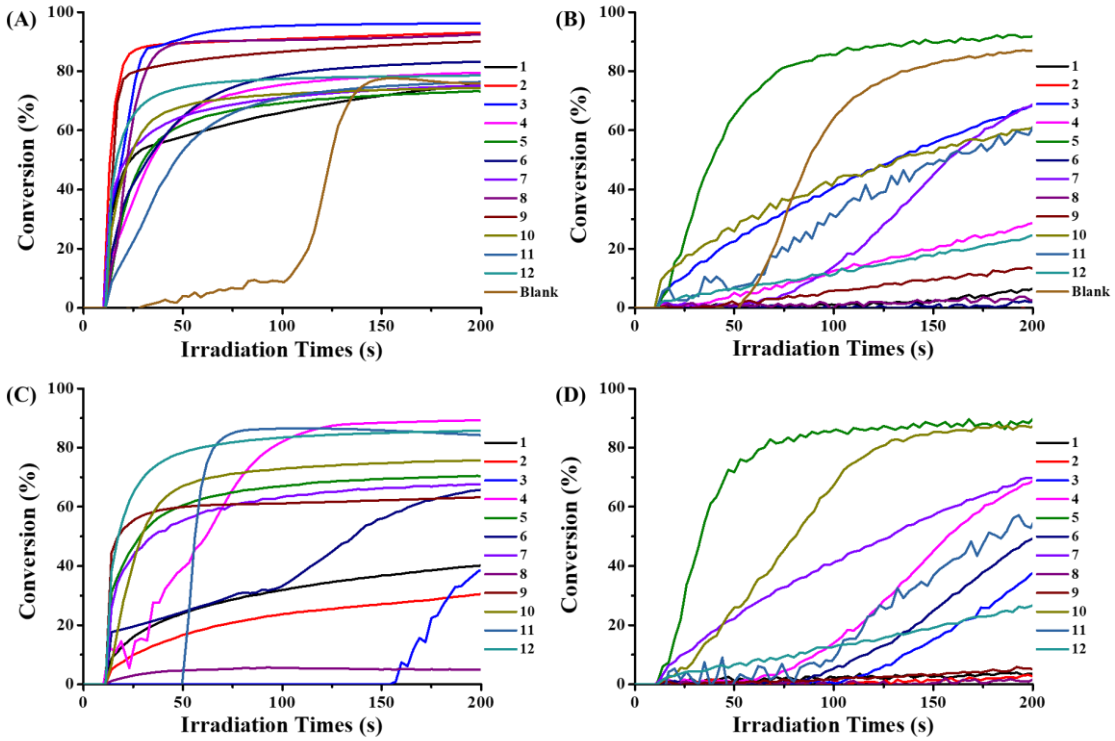

Figure 1. Photopolymerization profiles of PEG-DA (conversion of C=C bonds vs irradiation time) initiated by dyes/Iod/amine (0.1wt%/1.5wt%/1.5wt%, w/w/w) in laminate with different conditions, (A) irradiation by a LED@405nm (I_0 = 110

mW.cm^{-2}) with the thickness about 20μm; (B) irradiation by a LED@405nm (I_0 = 110 mW.cm^{-2}) with the thickness about 2mm; (C) irradiation by a LED@470nm (I_0 = mW.cm^{-2}) with the thickness about 20μm; (D) irradiation by a LED@470nm (I_0 = mW.cm^{-2}) with the thickness about 2mm, the irradiation starts form t =10s.

Final acrylate function conversions (FC) initiated by dye/Iod/amine				
Dyes	LED@405nm		LED@470nm	
	Thickness~20μm	Thickness~2mm	Thickness~20μm	Thickness~2mm
1	76%	7%	40%	-
2	93%	-	31%	-
3	96%	70%	39%	40%
4	80%	30%	89%	70%
5	73%	92%	70%	90%
6	83%	-	65%	50%
7	75%	70%	68%	70%
8	92%	-	5%	-
9	90%	13%	63%	-
10	75%	62%	76%	88%
11	76%	62%	84%	57%
12	79%	25%	86%	30%
Blank	76%	87%	-	-

'-' means not deep curing after irradiation for 200s

Table 2. Summary the FCs for the PEG-DA monomer while using dye/Iod/amine-based PISs with the thickness about 20μm and 2mm upon LED@405nm and LED@470nm. The blank corresponds iodonium/amine initiating systems without dyes.

3.2.2. Cationic polymerization (CP) kinetics of EPOX.

The initiating ability of the proposed dyes-based PIS for the CP of the EPOX were also studied upon irradiating with the LED @405nm in the air. As shown in Figure 2, the polymerization rate (the initial slope of the curves) of all dye-based PIS are much faster than that of blank PIS, while only the final conversion achieved by dye 6-based PIS is higher than that obtained by the blank PIS (92wt% of dye 6 *vs* 77wt% of blank, as shown in Table S1), which highlighting the crucial role of the three-component

systems for the overall performance. In addition, the thick samples can't deep curing, while the thin samples can be polymerized under the same condition. The efficiency of these PISs is determined by their photochemical reactivity with Iod and amine as well as the ability to generate radical cation ($dye^{\bullet+}$) (as shown in the chemical mechanisms below).

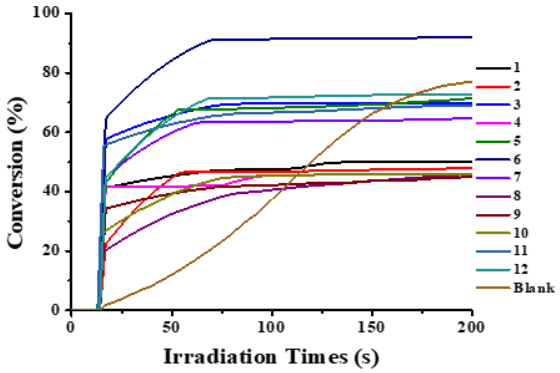

Figure 2. Photopolymerization profiles of EPOX (conversion of epoxy functions *vs* irradiation time) initiated by dyes/Iod/amine (0.1wt%/1.5wt%/1.5wt%, w/w/w) in the air upon irradiation with LED@405nm (I_0 = 110 $mW.cm^{-2}$) with the thickness of 20μm, the irradiation starts form t =10s.

3.2.3 Free Radical Polymerization (FRP) of PEG-DA Initiated by Dyes 3 and 5-based two-compound PISs or Dyes 3 and 5 alone as the PIs

In order to emphasize the important effect of the dye/Iod/amine based three-component PIS for the overall performance, the photoinitiation ability of the two-component PIS of i) dye 3 or 5/Iod (0.1wt%/1.5wt%, w/w) and dye 3 or 5/EDB (0.1wt%/1.5wt%, w/w) and ii) dye 3 or 5 alone used as PI (0.1wt%, w/w) for PEG-DA were also studied. As depicted in the Figure 3, deep curing can't be observed either for the thin samples or thick samples that only containing dyes 3 or 5 as PI. With the addition of Iod, the thick samples also can't deep curing, while the thin samples could be polymerized that the efficiency were slightly smaller than that achieved by the dyes 3 or 5/Iod/amine-based PISs (e.g. FCs ~90% of dye3/Iod *vs* ~96% of dye3/Iod/amine). Furthermore, with the addition of amine, the initiate ability of the thin sample of dye 3/amine was much smaller than that achieved by the dyes 3/Iod/amine-based PISs (FCs

~63% of dye3/amine *vs* ~96% of dye3/Iod/amine), while the thick sample of dye 3/EDB also can't deep curing. For the dye 5/EDB PIS, the polymerization efficiency of the thin samples and thick samples are slightly smaller than that obtained by dye 5/Iod/EDB-based PIS under the same conditions. The above results prove that the coexistence of dyes, Iod and amine has a huge effect on improving the efficiency of FRP for PEG-DA.

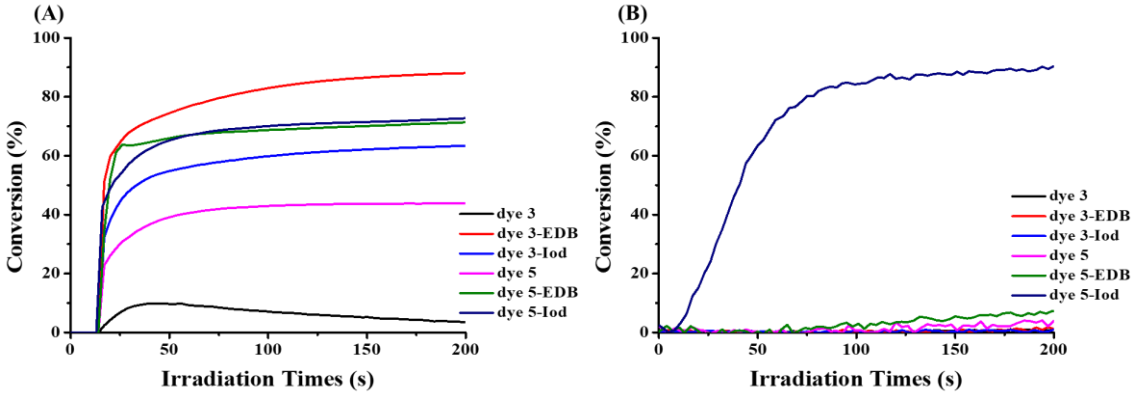

Figure 3. Photopolymerization profiles of PEG-DA (conversion of C=C bonds vs irradiation time) irradiation by a LED@405nm (I0 = 110 mW.cm^{-2}) with the thickness (A) about 20μm and (B) about 2mm, initiated by 0.1wt% dye 3, 0.1wt% dye 3/1.5wt% Iod, 0.1wt% dye 3/1.5wt% EDB, 0.1wt% dye 5, 0.1wt% dye 5/1.5wt% Iod as well as 0.1wt% dye 5/1.5wt% EDB. The irradiation time starts at t = 10 s.

3.2.4 3D printing experiments based on the proposed three-component PISs.

Since dyes 2, 3, 5, 8 and 9 were selected as excellent candidates to boost the FRP for PEG-DA and LED@405nm was selected as the light source, laser write experiments were carried out under these conditions. However, only dyes 3 and 5-based formulations could be successfully writen to obtain a stable 3D letter pattern ("**CZH**") with spatial resolution, and the morphologies were observed by the digital light microscopy which shown in Figure 4. Furthermore, all of them can be finished within 3 minutes , while it took shorter irradiation time for dye 5-based systems to get the 3D patterns than that of dye 3-based system.

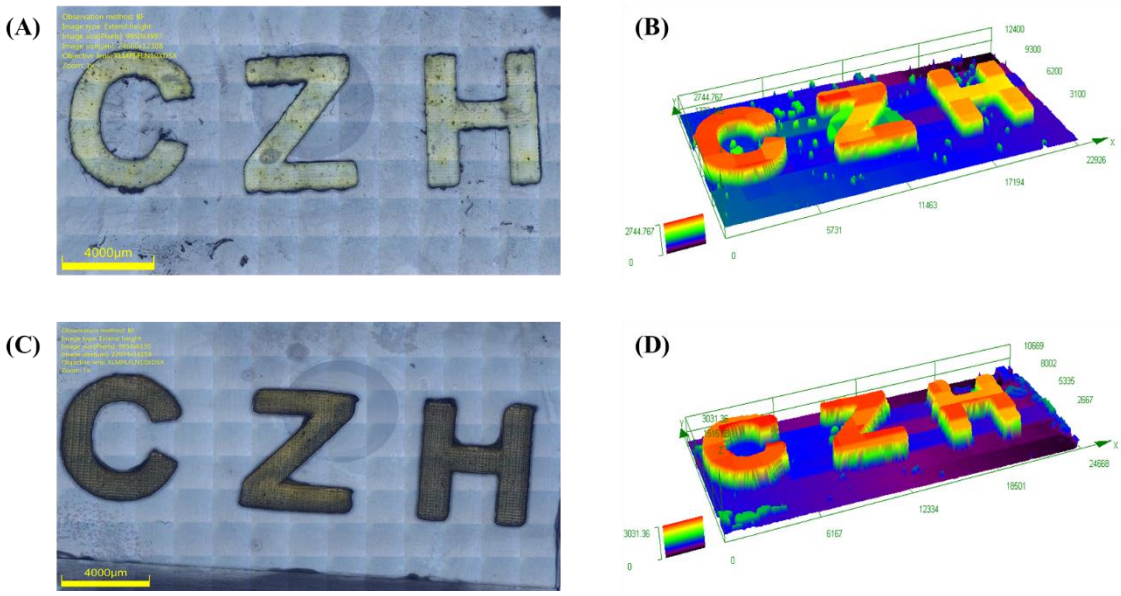

Figure 4. Free radical photopolymerization of PEG-DA through laser write experiments initiated by dyes-based PIS with LED@405nm. Characterization of the 3D patterns by numerical optical microscopy: (left) top surface morphology and (right) 3-D overall appearance: (a) (b) for dye 3-based PIS; (c) (d) for dye 5-based PIS.

3.3 Proposed Chemical Mechanisms

3.3.1 Steady state photolysis.

Steady-state photolysis of the dyes, dyes/Iod, dyes/amine as well as dyes/Iod/amine in acetonitrile have been carried out upon irradiation with a LED@405 nm. As evidenced by the UV-*vis* absorption spectra in Figure 5, obvious photolysis and significant declines of the absorption intensity were observed within 2 min. In the case of dye 3-based PIS, three changes can be observed for dye 3 alone during the photolysis process, but only the main absorption peak near 400nm is decreased with the light irradiation, and 15% consumption of dye 3 is achieved, which is closing to that achieved by the dye 3/EDB PIS that only the decrease of absorption peak at 400nm could be observed. Furthermore, two changes can be observed for the dye 3/Iod-based PIS, which achieved 35% consumption of dye 3, the main absorption peak near 400nm is decreased while the absorption peak around 350 nm increased with the light

irradiation. The dye/Iod/amine-based PIS achieved the highest consumption of dyes (~42%) within 120 s and the main absorption peak near 400 nm was also decreased.

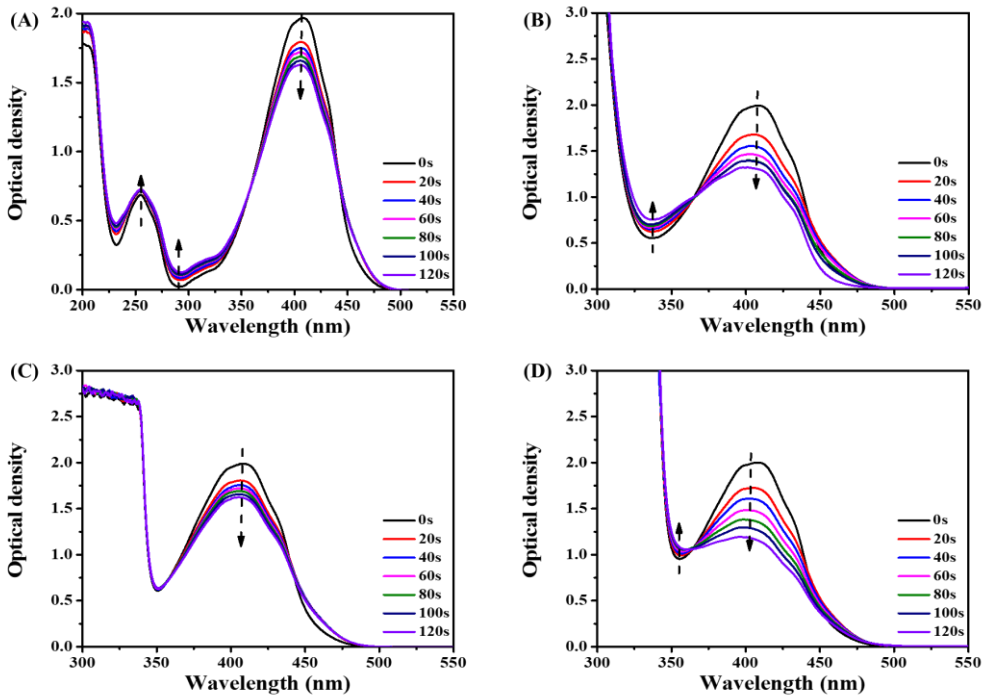

Figure 5. Photolysis of (A) dye 3; (B) dye 3/Iod; (C)dye 3/amine and (D) dye 3/Iod/amine upon exposure to LED@405nm under air in acetonitrile.

Remarkably, the photolysis process of the dye 5-based one/two or three-compound PISs were different to those of dye 3-based PISs, which shown in Figure 6, and the consumptions of dye 5 were summarized in Figure S2. The dye5/Iod- and dye 5/Iod/amine-based PIS exhibited a rapid photolysis that the main absorption peak near 450nm appeared a blue-shift and disappeared within 25s, and these two PISs reached about 80% consumption of dye 5. However, there were no obvious photolysis for the dye 5- and dye 5/amine-based PISs, which just realized 5% consumption of dyes within 25s. Since the speed of the photolysis process depends on the ability of the electron transfer between the dyes with the Iod or amine, the above photolysis results prove that dye 5 with Iod and amine exhibited higher electron transfer efficiency than that of dye 3, which is completely related to the additional amine group contained in the structure of dye 5.

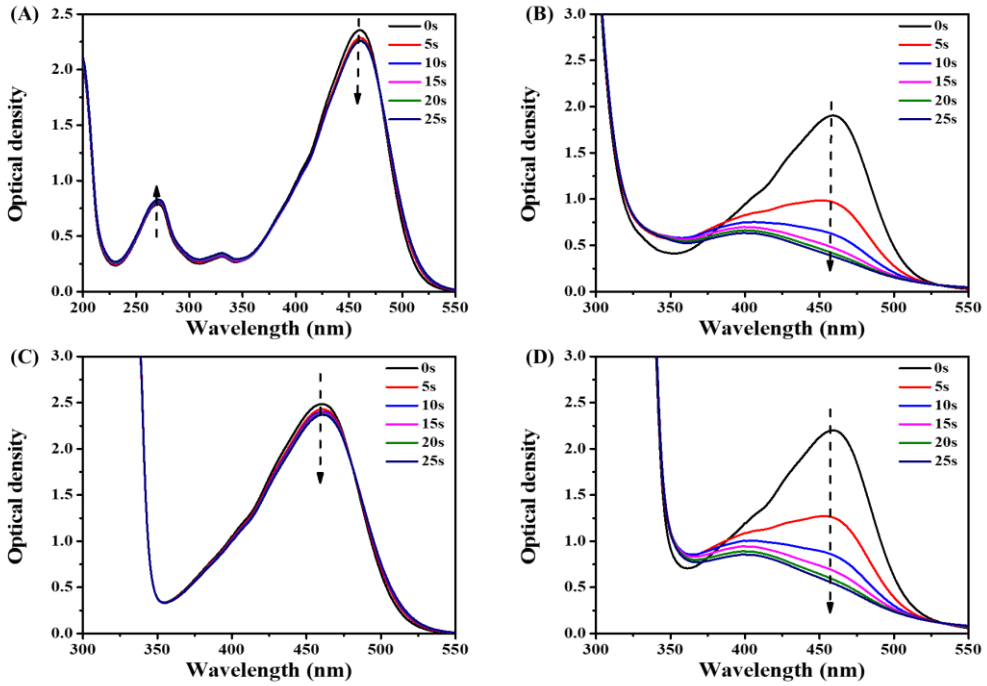

Figure 6. Photolysis of (A) dye 5; (B) dye 5/Iod; (C)dye 5/amine and (D) dye 5/Iod/amine upon exposure to LED@405nm under air in acetonitrile.

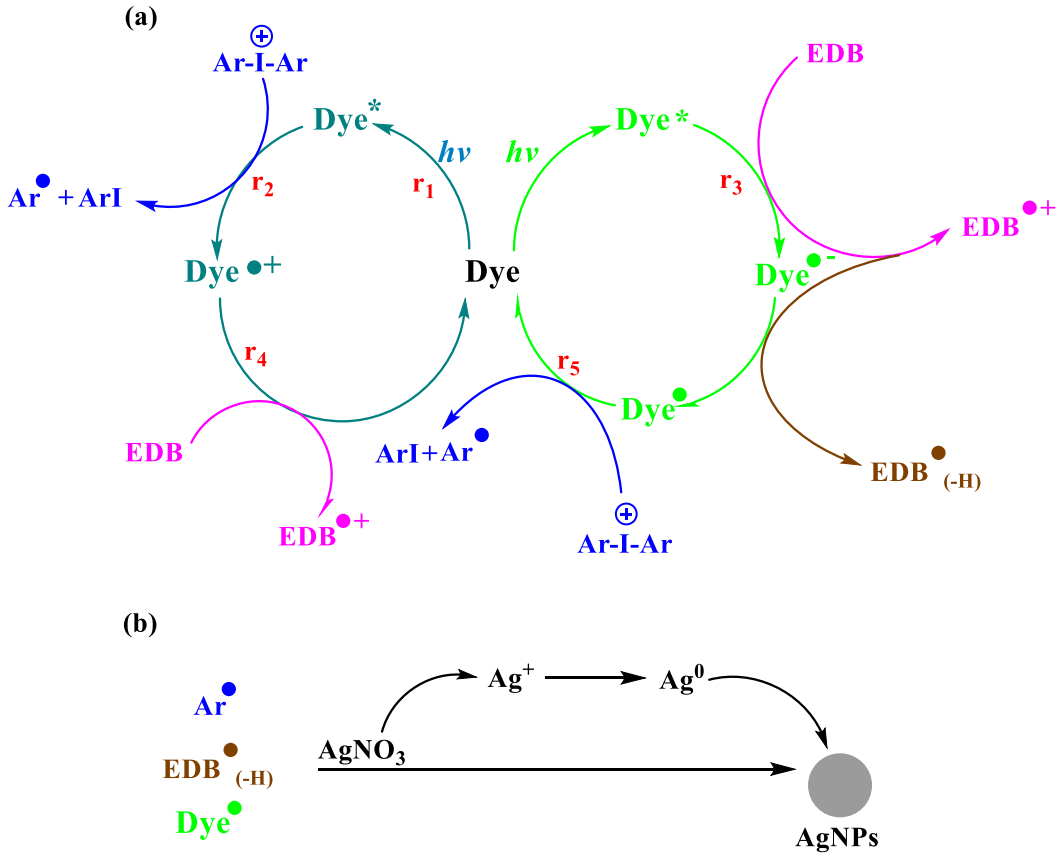

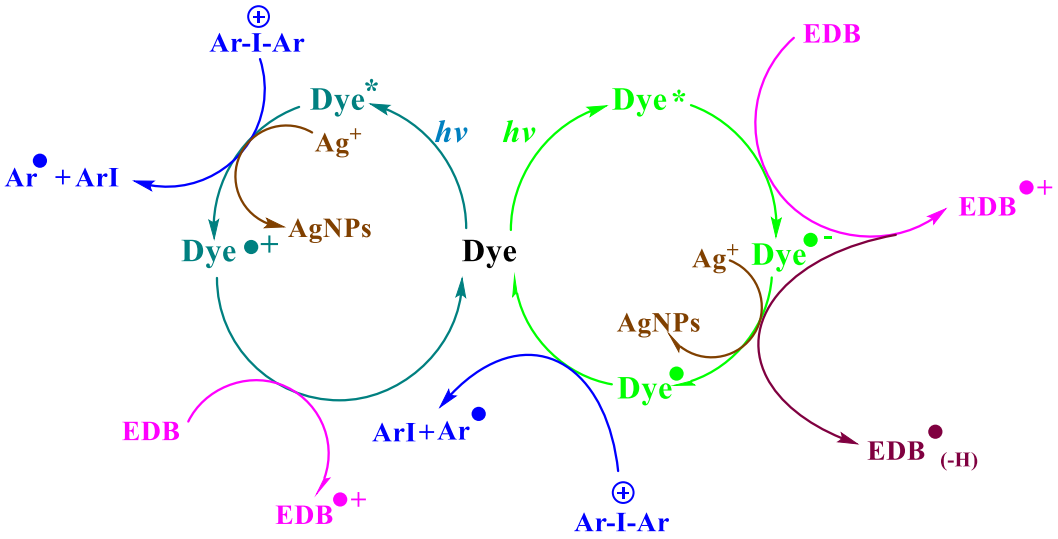

Scheme 3. (a) Proposed photoinitiation step mechanisms of dyes/Iod/amine initiating systems; (b) Photoinitiation mechanism of dyes/Iod/amine with metallic salts in air atmosphere.

3.3.2 Fluorescence quenching experiments.

The emission and fluorescence quenching spectra of dye 3 and 5 in acetonitrile were recorded and the different curves are presented in Figure S3. The addition of Iod or amine all clearly exhibited a decrease in the emission intensity of dye 3 and 5, which showed that the Iod and the amine can act as good quenchers since the interaction between the dye with Iod or amine in the excited singlet state. Remarkably, a linear curve can be fitted from the fluorescence quenching processes between the dyes with Iod. Furthermore, the value of the Stern-Volmer coefficients (K_{SV}, the slope of the curve, Table 3) as well as the electron transfer quantum yield (ϕ_{et}, Table 3) for the expected electron transfer reaction between the dyes and Iod or amine can be calculated by the equation 5, which also showed the favorable fluorescence quenching processes of the excited singlet states by Iod or amine [30,31].

$$\Phi_{et} = K_{sv} * [\text{Iod/amine}] / (1 + Ksv * [\text{Iod/amine}]) \quad (5)$$

The theoretical feasibility of the interactions between dye/Iod (or dye/amine) was investigated by calculating the free energy changes of the electron transfer reactions (ΔG_{Iod} or ΔG_{EDB}, respectively). The first singlet excited state energy (E_{S1}) can be

defined through the point of intersection between the absorption and the fluorescence spectra (e.g. E_{S1} = 2.74 eV and 2.50 eV for dye 3 and dye 5, respectively; Table 5). The oxidation potential and the reduction potential of dyes 3 and 5 was studied through the cyclic voltammetry experiments. As shown in Figure 7, two oxidation peaks can be observed in the positive potential range of dye 5, which corresponds to further oxidation (irreversible) even at higher potentials. In addition, clear reduction peaks were also observed. For the dye 3, a clear oxidation peak and a reduction peak can be observed in this cycle. According to the equations (1) or (2), ΔG_{Iod} or ΔG_{EDB} were determined from the oxidation potential E_{ox} (or from the reduction potential $E_{red)}$, and the first singlet excited state energy (E_{S1}) that all of them are all less than 0 except the ΔG_{EDB} of dye 5 was 0. All these results revealed that the electron transfer reactions can be occurred between dyes/Iod and dyes/amine.

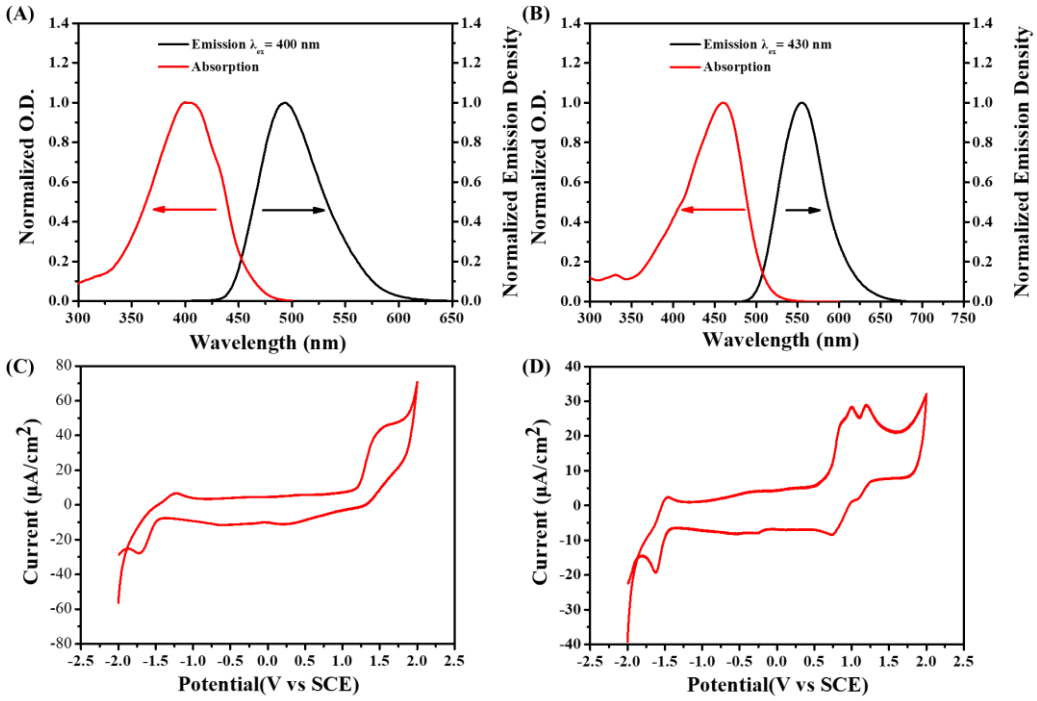

Figure 7. Singlet state energy of (A) dye 3; (B) dye 5 determinated in acetonitrile and the cyclic voltammetry of electrochemical reactions of (C) dye 3 and (D) dye 5 in acetonitrile solvent against saturated calomel electrode (SCE) under N_2 saturated solution.

	Dye 3	**Dye 5**

K_{sv}^{Iod} (M^{-1})	93	58
Φ_{et}^{Iod}	11	10
K_{sv}^{Amine} (M^{-1})	0.16	0.11
Φ_{et}^{Amine}	0.06	0.055
E_{S1}（eV）	2.74	2.50
E_{ox}（eV）	1.33	0.79
E_{red}（eV）	-1.60	-1.50
ΔG^{S1}_{Iod}	-0.71	-1.01
ΔG^{S1}_{EDB}	-0.14	0

Table 3. Parameters characterizing the fluorescence properties of dye 3 and 5 in acetonitrile: Interaction constant (Ksv) of dye-Iod and dye-EDB systems calculated by Stern-Volmer equation; electron transfer quantum yield (Φ^{et}) of dye/Iod and dye//EDB interactions; singlet excited state energy (E_{S1}); oxidation potential (E_{ox}) and reduction potential (E_{red}) measured by Cyclic Voltammetry experiments as well as free energy change of singlet electrode (ΔG_{S1}).

3.4.4 ESR experiments of dye 5–based photoinitiating system

The ESR-spin trapping experiments were successfully performed under N_2 to detected the generated radicals from the dye 5/ Iod and dye 5/amine solutions. As shown in the Figure S4 (A) and (B), the phenyl radicals were captured within the dye 5/ Iod that are depicted by the hyperfine coupling constants for nitrogen and hydrogen: a_N = 14.4 G and a_H = 2.2 G, which are completely consistent with the literature [32] and also proved the occurrence of interaction between dye and Iod showing in Scheme 3. Furthermore, the a_N = 14.4 G and a_H = 2.2 G detected from the dye 5/amine solution (Figure S4 (C) and (D)) evidenced the generation of aminoalkyl radicals according to experimental data published elsewhere (a_N = 14.4 G and a_H = 2.2 G, [33]).

3.4. AgNPs in DMF Solution and PEG-polymers.

In this study, through redox reactions between dyes used as photoinitiators and the additive Iod/amines, a series of free radicals and cations were generated with the irradiation of LED@405nm (as shown in Scheme 3), which have two roles, one is to induce the polymerization of PEG-DA monomers, and the other is to reduce the metal salt in to AgNPs *in situ*. The AgNPs generated in DMF solution can be indicated through the UV-*vis* absorption spectra and the change of color of the solution. As given in Figure 8 (A), two absorption peaks at 400 nm and 460 nm were observed and the absorption peak at 460nm was decreased since the photolysis of dye 5 while the absorption peak at 400nm was increased due to the generation of AgNPs after irradiation for 90 min. Moreover, the color of the solution changed from light brown to dark brown and even one side of the cuvette turned into silver color as the coating by silver nanoparticles (see in Figure 8 (B)).

Furthermore, the AgNPs generated in PEG-polymers were characteristed through the changes of the color of the PEG-monomer polymerized upon irradiation with LED@405nm (see in Figure 8 (D)) which followed by the RT-FTIR. The color also changed from light brown to dark brown, while the same changes can also be observed when coating thin films from 4 layers to 20 layers. However, although the polymerization efficiency of the formulation containing AgNPs shown in Figure 8 (C) is lower than that obtained for the formulation without AgNPs, its final acrylate function conversion rate is still about 80% after irradiation for 300s.

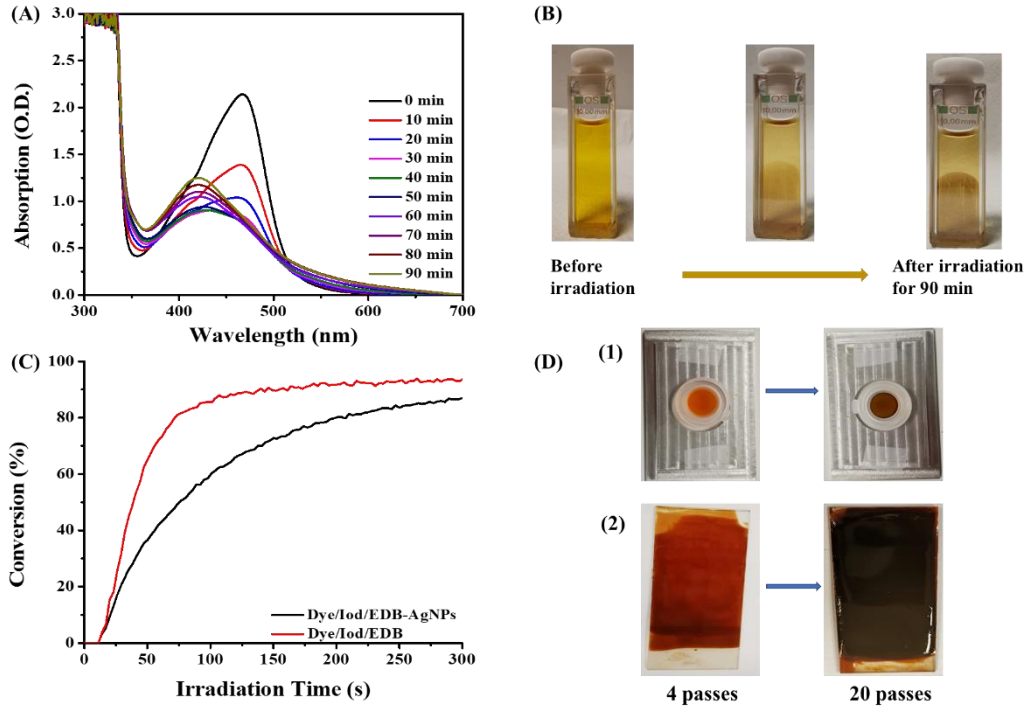

Figure 8. (A) In-situ preparation of AgNPs with dye 5/Iod/EDB (0.05 wt%) and $AgNO_3$ (4 wt%) in DMF followed by UV-*vis* absorption spectroscopy in air atmosphere; (B) the color of solution turned to dark brown after 90 minutes light irradiation; (C) photopolymerization profiles of PEG-DA (conversion rate of C=C bonds vs irradiation time) containing AgNPs initiated by dye 5/Iod/amine upon exposure to a LED@405nm in laminate. The irradiation starts for t =10s; (D) The color changes of PEG-polymers containing $AgNO_3$.

The size and the shape of the AgNPs generated in DMF solution and PEG-polymers were detected by TEM and the images were given in Figure 9. The AgNPs in DMF are irregularly spherical with the size of about 2~4 nm, while the AgNPs in PEG-polymer are in a regular spherical shape with the size varied from 20~40nm, which are much larger than that obtained in DMF since they aggregated.

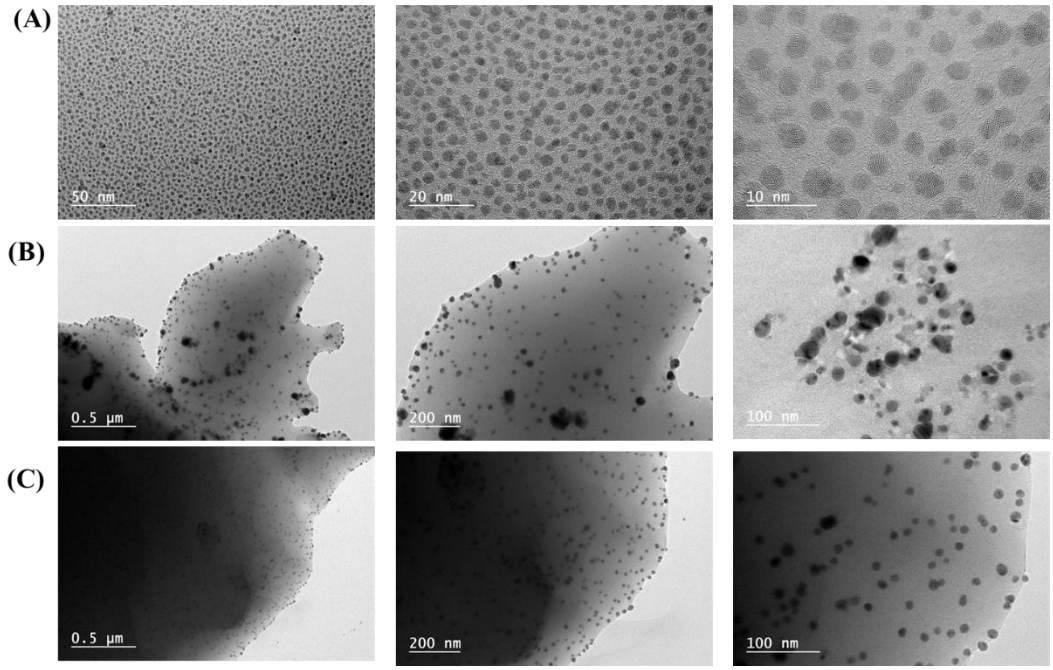

Figure 9. TEM images of (A) AgNPs prepared in DMF solution; (B) AgNPs prepared in PEG-polymer from FTIR experiment; (c) AgNPs prepared in 20 layers of PEG-polymer films.

3.5 Applications in 4D

3.5.1 Swelling experiment of PEG-polymers with/without AgNPs.

The swelling ratios of the PEG-polymers with/without AgNPs that initiated by the three-component PISs based on dyes 3 or 5/Iod/amine (0.1wt%/1.5wt%/1.5wt%) were investigated. As shown in Figure 10, after immersing the polymers in water to reach the swelling equilibrium, the swelling ratio of the polymers without AgNPs were about 70wt%-90wt%, and their volumes increased about 170wt%-190wt% (see in Table 5) than its primary. However, the swelling ratio of the AgNPs-containing polymers were about 60wt% and the ratio of their volume increased were about 150wt%-160wt%, which were smaller than that achieved by the polymers without AgNPs. This may be due to the decrease of the crosslink density of the polymers since the generation of AgNPs. Subsequently, the polymers that reached swelling equilibrium were heated in an oven at 50°C for 1h to remove the contained-water, they returned to their original weight and volume (as shown in Figure 10(B)), while the shape was a little deformed, indicating that the swelling behavior of these polymers are reversible.

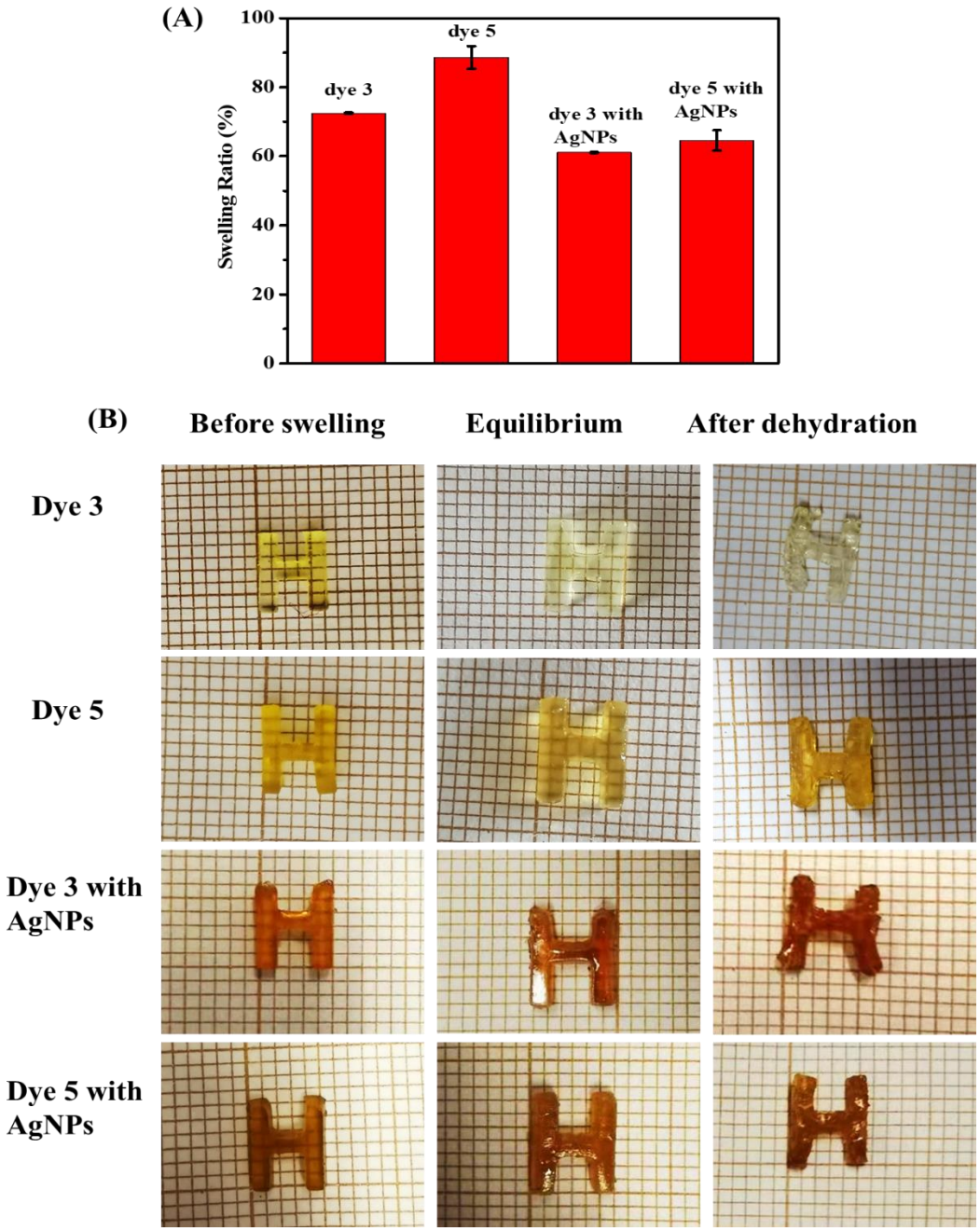

Figure 10. (A) the swelling ratio of PEG-polymer with/without AgNPs prepared using dye/Iod/amine; (B) the photos of PEG-polymer with/without AgNPs initiated by dye/Iod/amine before water swelling, after water swelling for 24h and after heating for 1h to remove water.

	Dye 3	**Dye 5**	**Dye 3 with AgNPs**	**Dye 5 with AgNPs**
V_1 (mm^3)	39.39	42.74	27.97	31.11

V_2 (mm^3)	69.32	81.23	40.27	49.60
V_3 (mm^3)	38.12	34.98	16.28	30.40
R (%)	176wt%	190wt%	144wt%	160wt%

Table 4. The 3D pattern volumes for the comparison in the cycle: before water swelling (V_1), swelling equilibrium (V_2), after heating (V_3) as well as the increase ratio of volume after swelling (*R*).

3.5.2 The reversible deformation effect of PEG-polymer with/without AgNPs.

The combination of the proposed dye 5/Iod/amine based PIS and PEG-DA can be used for 3D bioprinting as the high biocompatibility and hydrophilicity of PEG polymers. According to my previous study [34], the reversible deformation effect of PEG-polymers is associated with the irradiation time, so we chose the best irradiation time to prepare a cross object with spatial resolution characteristics and detect its 4D deformation effect *via* swelling and dehydration. Subsequently, the influence of silver nanoparticles on the 4D deformation properties of PEG-polymers is also studied by comparing the shapes change performance of PEG-polymers with/without AgNPs. As shown in Figure 11(A)/(B) -1, the color of the cross containing AgNPs is darker than the polymer without the AgNPs. After soaked in a water filled beaker, these two polymers all curled as swelling in water, while the degree of deformation of the polymer without AgNPs is greater than that of the polymer containing nanoparticles (Figure 11 (A)/(B)-2 and SI Video 1 or 3). Subsequently, the polymers removed from water and heated at 80°C to dehydrated. Correspondingly, the curled cross flattened out and returned to its original shape after 5 mins as the contained water removed (Figure 11 (A)/(B)-3 and SI Video 1 or 3). Then the continuous heating for 10 minutes to completely dehydrate the cross could makes them curled upside down as shown in Figure 12 (A)/(B)-4 and the degree of deformation of the polymer containing AgNPs is also smaller than that of the polymer without nanoparticles. Finally, removed the curled polymers into room temperature, the curled polymers were gradually flatted out or even returned to its primary shape (see Figure 11 (A)/(B)-5). Figure 11(A)/(B)-6 to 8 shows the second deformation process of these two polymers, which demonstrated that the available hydrogels initiated by the new PIS based on dye 5/Iod/amine have a reversible

deformation effect due to its thermal- and water- responsiveness of PEG and the presence of AgNPs in PEG-polymers will reduce the degree of 4D deformation [35-37].

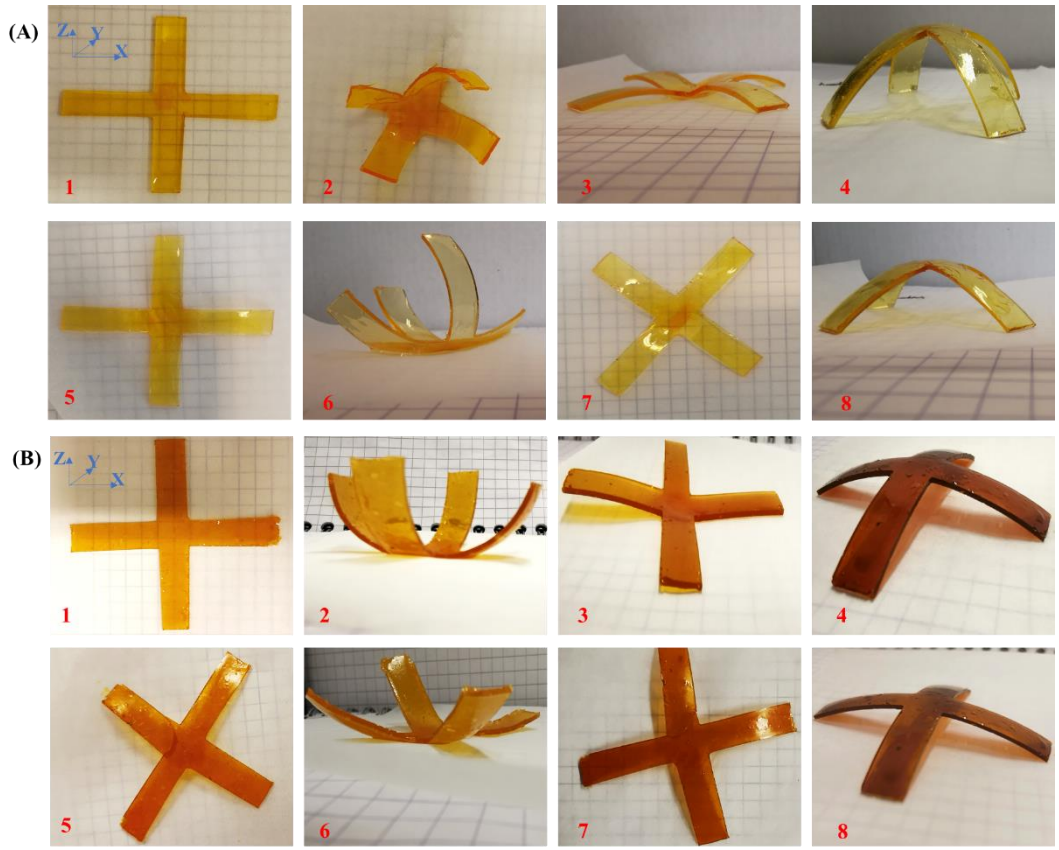

Figure 11. (A) Swelling and dehydration induced actuation of (A) PEG-polymer and (B) PEG-polymer containing AgNPs initiated by dye5/Iod/amine irradiation with LED@405 nm: (1) cross of PEG-polymer after 1min light irridiation, (2) cross after water swelling for 1 min (see SI Video 1 or 3), (3) cross after 100 seconds of dehydration (heating at 100 ℃, see SI Video 1 or 3), (4) cross after 10 mins of dehydration (heating at 100 ℃), (5) cross after stay at room temperature for 10 mins; (6) cross after water swelling again for 1 min (see SI Video 2 or 4); (7) cross after 100 seconds of dehydration (heating at 100 ℃, see SI Video 2 or 4), (8) cross after 10 mins of dehydration (heating at 100 ℃).

4. Conclusions

In conclusion, twelve different dyes with 2,5-diethylene-cyclopentane-1-one as the main structure were synthesized and used as photoinitiators with the combination of Iod and EDB. Under LED irradiation, the oxidation–reduction reactions could take place between dyes and Iod/EDB, which generate free radicals and cations to induce

the polymerization of PEG-DA/EPOXY monomer, furthermore, it can also reduce the metal salt into AgNPs. As the π-conjugation in the molecular structures, all these dyes displayed strong absorption in the near UV or visible range, which in agreement with their excellent polymerization efficiency for the free radical polymerization and the cationic polymerization. Remarkably, dyes 3 and 5 proved to be the excellent photoinitiators. The steady state photolysis, fluorescence quenching as well as ESR-ST experiments were successfully performed to characterized the involved photochemical mechanisms. Finally, the PEG-polymers with reversible deformation effect can also be observed and the generation of AgNPs could reduce their swelling and 4D deformation performance. In addition, the above-mentioned photocurable resin with the thermal- and water-response can potentially be used in emerging fields including biomedical engineering, smart response materials, etc.

Supplementary Materials:

The following are available online

Acknowledgments: This research project is supported by China Scholarship Council (CSC) 201906280059. The DGA is acknowledged for its financial support through the PhD grant of Damien Brunel. This research was also funded by the Agence Nationale de la Recherche (ANR agency) through the PhD grant of Guillaume Noirbent (ANR-17-CE08-0054 VISICAT project). P. X. acknowledges funding from the Australian Research Council (FT170100301). This work was granted access to the HPC resources of the Mesocentre of the University of Strasbourg.

Conflicts of Interest:

The authors declare no conflict of interest.

References

(1) Aleksandra S.; Murielle O.; Marine D.; Loïc V.; Lavinia B. Photo-induced design of reflective metallized gold@polymer coatings with tuned architecture. *Materials and Design.* **2018**, *160*, 74-83.

(2) P. Rafighi, M. Tavahodi, B. Haghighi, Fabrication of a third-generation glucose biosensor using graphene-polyethyleneimine-gold nanoparticles hybrid. *Sensors Actuators B Chem.* **2016**, *232*, 454-461.

(3) Yue G, Su S, Li N, Shuai M, Lai X, Astruc D, Zhao P. Gold nanoparticles as sensors in the colorimetric and fluorescence detection of chemical warfare agents. *Coord. Chem. Rev.* **2016**, *311*, 75-84.

(4) M.-R. Zhang, X.-Q. Chen, G.-B. Pan, Electrosynthesis of gold nanoparticles/porous GaN electrode for non-enzymatic hydrogen peroxide detection. *Sensors Actuators B Chem.* **2017**, *240*,142-147.

(5) Shenashen, M.; El-Safty, S.; Elshehy, E. Synthesis, Morphological Control, and Properties of Silver Nanoparticles in Potential Applications. *Part. Part. Syst. Charact* **2014**, *31*, 293-316.

(6) Fahr, S.; Rockstuhl, C., Lederer, F. Metallic nanoparticles as intermediate reflectors in tandem solar cells. *Appl. Phys. Lett.* **2009,** *95*, 121105.

(7) Y. Chaikin, O. Kedem, J. Raz, A. Vaskevich, I. Rubinstein, Stabilization of Metal Nanoparticle Films on Glass Surfaces Using Ultrathin Silica Coating. *Anal. Chem.* **2013**, *85*, 10022-10027.

(8) S. Iravani, H. Korbekandi, S.V. Mirmohammadi, B. Zolfaghari1. Synthesis of silver nanoparticles: chemical, physical and biological methods. *Res Pharm Sci.* **2014,** 9, 385-406.

(9) H. Tyagi, A. Kushwaka, A. Kumar, M. Aslam, Magnetic Behavior of Surface Nanostructured 50-nm Nickel Thin Films. *Nanoscale Res. Lett.* **2016,** *11*, 362.

(10) L. Malassis, R. Dreyfus, R.J. Murphy, L.A. Hough, B. Donnio, C.B. Murray. One-step green synthesis of gold and silver nanoparticles with ascorbic acid and their versatile surface post-functionalization. *RSC Adv.* **2016**, *6*, 33092-33100.

(11) A. Jimenez-Ruiz, P. Perez-Tejeda, E. Grueso, P.M. Castillo, R. Prado-Gotor, Nonfunctionalized Gold Nanoparticles: Synthetic Routes and Synthesis Condition Dependence. *Chem. Eur. J.* **2015**, *21*, 9596-9609.

(12) T.K. Sau, A.L. Rogach, Nonspherical noble metal nanoparticles: colloid-chemical synthesis and morphology control. *Adv. Mater.* **2010**, *22*, 1781-1804.

(13) Zhu, SQ., Zhang, T., Guo, XL. et al. Gold nanoparticle thin films fabricated by electrophoretic deposition method for highly sensitive SERS application. *Nanoscale. Res. Lett.* **2012**, *7*, 613-620.

(14) Mohamed Zaier, Loïc Vidal, Samar Hajjar-Garreau & Lavinia Balan. Generating highly reflective and conductive metal layers through a light-assisted synthesis and assembling of silver nanoparticles in a polymer matrix. *Scientific Reports*. **2017**, *7*, 12410-12417.

(15) Cornelissen, J.J.L.M., Heerbeek, R., Kamer, P.C.J., Reek, J.N.H., Sommerdijk, N.A.J.M., Nolte, R.J.M. Silver nanoarrays templated by block copolymers of carbosilane dendrimers and polyisocyanopeptides. *Adv. Mater.* **2002**, *14*, 489-492. (2002).

(16) Balan, L.; Schneider, R.; Lougnot, D. J. In situ fabrication of polyacrylate-silver nanocomposite through photoinduced tandem reactions involving eosin dye. *Prog. Org. Coat.* **2008**, *62*, 351-357.

(17) Ali Bagheri, A.; Jianyong Jin, J.Y. Photopolymerization in 3D Printing. *ACS Appl. Polym. Mater*. **2019**, *1*, 593-611.

(18) Zhang, J.; Hill, N.; Lalevee, J.; Fouassier, J.-P.; Zhao, J.; Graff, B.; Schmidt, T.-W.; Kable, S.-H.; Stenzel, M.-H.; Coote, M.-L.; Xiao, P., Multihydroxy-anthraquinone derivatives as free radical and cationic photoinitiators of various photopolymerizations under green LED. Macromol. Rapid. Commun. 2018, 39, e1800172.

(19) J. Fouassier, Lalevée, J. Photopolymerization upon LEDs: new photoinitiating systems and strategies. *Polym. Chem.* **2015**, *6*, 3895-3912.

(20) Alexandridis, P.; Tsianou, M. Block copolymer-directed metal nanoparticle morphogenesis and organization. *Eur. Polym. J.* **2011**, *47*, 569-583.

(21) Chen, H.; Noirbent, G.; Sun, K.; Brunel, D.; Gigmes, D.; Morlet-Savary, F.; Zhang, Y.J.; Liu, S.H.; Xiao, P.; Dumur, F.; Lalevée, J. Photoinitiators derived from natural product scaffolds: monochalcones in three-component photoinitiating systems and their applications in 3D printing. *Polym. Chem.*, **2020**,*11*, 4647-4659.

(22) Paul, C.B.; David, G. studies of Rhodamine 6G, Rhodamine B and Rhodamine. *J.*

Chem. Soc., Faraday Trans., **1993**, *89*, 4185-4191.

(23) Rehm, D.; Weller, A. Kinetics of fluorescence quenching by electron and H-atom transfer. *Isr. J. Chem.* **1970**, *8*, 259-271.

(24) Sun, K.; Xu, Y.Y.; Dumur, F.; Morlet-Savary, F.; Chen, H.; Dietlin, C.; Graff, B.; Lalevée, J.; Xiao, P. In silico rational design by molecular modeling of new ketones as photoinitiators in three-component photoinitiating systems: application in 3D printing. *Polym. Chem.*, **2020**,*11*, 2230-2242.

(25) Duling, D.-R. Simulation of multiple isotropic spin-trap EPR spectra. J. Magn. Reson. 1994, 104, 105-110.

(26) Mutlu, S.; Metin. E.; Yuksel, S.A.; Bayrak, U.; Nuhoglu, C.; Arsu. N. In-situ photochemical synthesis and dielectric properties of nanocomposite thin films containing Au, Ag and MnO nanoparticles. *Eur. Polym. J.* **2021,** 144, 110238.

(27) Chen, H.; Noirbent, G.; Zhang, Y.J.; Brunel, D.; Gigmes, D.; Morlet-Savary, F.; Gigmes, D.; Xiao, P.; Dumur, F.; Lalevée, J. Novel D–π-A and A–π-D–π-A three-component photoinitiating systems based on carbazole/triphenylamino based chalcones and application in 3D and 4D printing. *Polym. Chem.*, **2020**, *11*, 6512-6528.

(28) Shen, Y.M.; Wang, H.; Liu, Z.J. Li, W.K.; Liu, Y.H.; Li, J.J.; Wei, H.L.; Han, H.Y. Fabrication of a water-retaining, slow-release fertilizer based on nanocomposite double-network hydrogels via ion-crosslinking and free radical polymerization. *J. Ind. Eng. Chem.* **2021**, *93*, 375-382.

(29) Theoretical Description of Hydrogel Swelling: A Review. *Iran. Polym. J.* **2010**, *19*, 375-398.

(30) Zeng, H.L.; Durocher, G. Analysis of fluorescence quenching in some antioxidants from non-linear Stern—Volmer plots. *J. Lumin.*, **1995**, *63*, 75-84.

(31) Langer, G.; Berer, T. Fluorescence quantum yield and excited state lifetime determination by phase sensitive photoacoustics: concept and theory. *Opt. Lett.* **2018**, *43*, 5074-5077.

(32) Lalevée, J.; Tehfe, M.A.; Zein-Fakih, A.; Ball, B.; Telitel, S.; Morlet-Savary, F.; Graff, B.; Fouassier, J.P. N-Vinylcarbazole: An Additive for Free Radical

Promoted Cationic Polymerization upon Visible Light. *ACS. Macro. Lett.* **2012**, *1*, 802-806.

(33) Lalevée, J.; Gigmes, D.; Bertin, D.; Graff, D.; Allonas, X.; Fouassiera, J.P. Comparative reactivity of aminyl and aminoalkyl radicals. *Chem. Phys. Lett.* **2007**, *438*, 346-350.

(34) Chen, H.; Zhang, Y.J.; Bonfiglio, A.; Morlet-Savary, F.; Mauro, M.; Lalevée, J. Rhenium(I) N-Heterocyclic Carbene Complexes in Photoinitiating Systems for Polymerization upon Visible Light: Development of Photosensitive Resins for 3D and 4D Applications. *ACS. Appl. Polym. Master.* **2021**, *3*, 464-473.

(35) Liu, Y.; Li, Y.; Yang, G.; Zheng, X.T.; Zhou, S.B., Multi-Stimulus-Responsive Shape-Memory Polymer Nanocomposite Network Cross-Linked by Cellulose Nanocrystals. *ACS Appl. Mater. Interfaces.* **2015**, *7*, 4118-4126.

(36) Liu, C.D.; Chun, S.B.; Mather, PT. Chemically Cross-Linked Polycyclooctene: Synthesis, Characterization, and Shape Memory Behavior. *Macromolecules.* **2002**, *35*, 9868-9874.

Supporting Information

In-situ Generation of Ag Nanoparticles during Photopolymerization and the 3D/4D Applications through

Using Newly Developed Dyes-Based Three-Component Photoinitiating Systems

Hong Chen [1,2], Sun ke [1,2], Yijun Zhang [1,2], Fabrice Morlet-Savary [1,2], Pu Xiao [4*], Frédéric Dumur [3*], Jacques Lalevée [1,2*]

[1] Université de Haute-Alsace, CNRS, IS2M UMR 7361, F-68100 Mulhouse, France; jacques.lalevee@uha.fr
[2] Université de Strasbourg, France
[3] Aix Marseille Univ, CNRS, ICR UMR 7273, F-13397 Marseille, France ; frederic.dumur@univ-amu.fr

[4] Research School of Chemistry, Australian National University, Camberra, ACT 2601, Australia; pu.xiao@anu.edu.au

* Corresponding author: jacques.lalevee@uha.fr (J. L.), frederic.dumur@univ-amu.fr (F.D.); pu.xiao@anu.edu.au (P. X.).

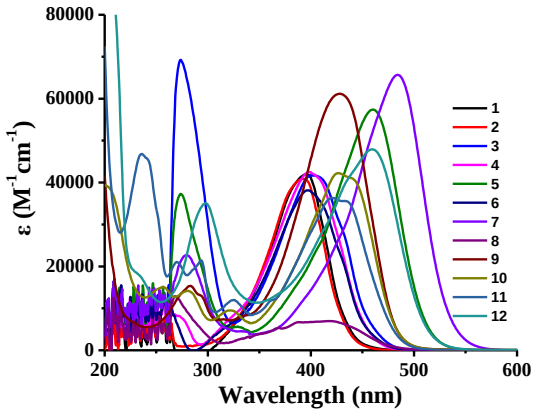

Figure S1. The UV-*vis* absorption spectra of dyes 1-12 in acetonitrile.

Final epox function conversions (FC) initiated by dye/Iod/amine							
Dyes	1	2	3	4	5	6	7
FCs	50%	48%	70%	46%	72%	92%	65%
Dyes	8	9	10	11	12	Blank	
FCs	46%	45%	46%	69%	73%	77%	

Table S1. Summary of the FCs for the EPOX monomer dye/Iod/amine-based PISs with the thickness about 20μm upon LED@405nm.

Final acrylate function conversions (FC) initiated by dyes 3 and 5-based PIS							
Thickness ~20μm	**Dyes**	3	3-Iod	3-EDB	5	5-Iod	5-EDB
	FCs (wt%)	-	88wt%	63wt%	-	71wt%	73wt%
Thickness ~2mm	**Dyes**	3	3-Iod	3-EDB	5	5-Iod	5-EDB
	FCs (wt%)	-	-	-	-	-	89wt%

Table S2. Summary the FCs for the PEG-DA monomer upon irradiation with a LED@405 nm that initiated by 0.1wt% dye 3, 0.1 wt% dye 3/1.5 wt% Iod, 0.1 wt% dye 3/1.5 wt% EDB, 0.1 wt% dye 5, 0.1wt% dye 5/1.5wt% Iod as well as 0.1wt% dye 5/1.5wt% EDB in laminate.

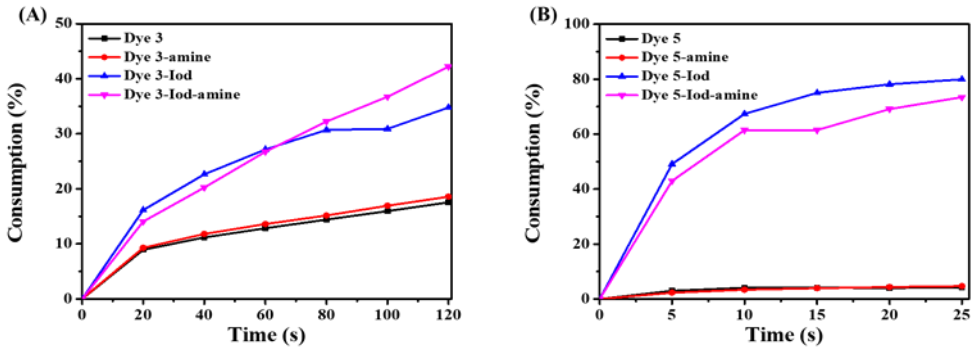

Figure S2. The consumption of (A) dye 3 and (B) dye 5 during the photolysis process.

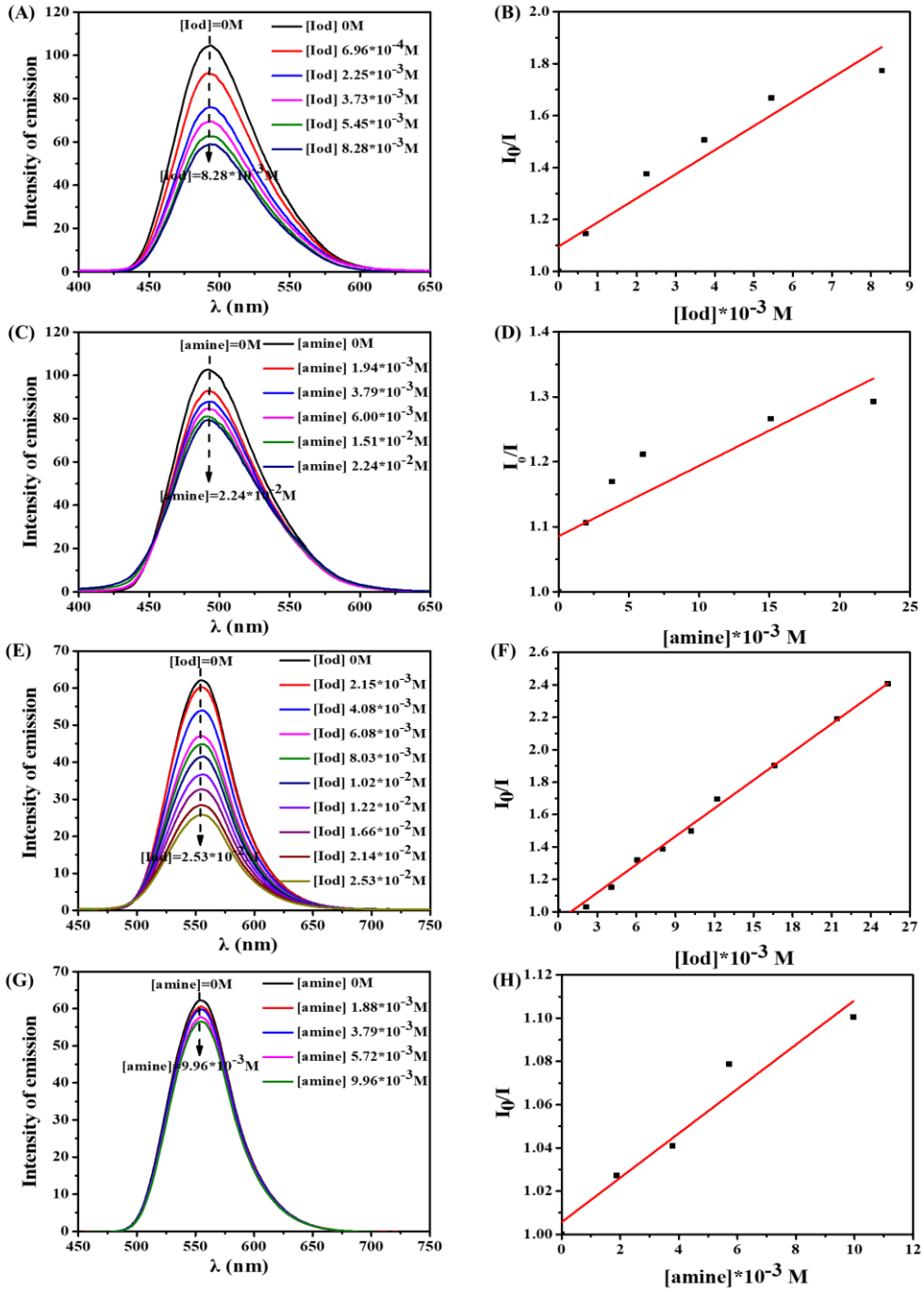

Figure S3. (A) Fluorescence quenching of dye 3 by Iod (speedcure 938); (B) Stern-Volmer treatment for the dye 3/Iod fluorescence quenching; (C) Fluorescence quenching of dye 3 by amine (speedcure EDB); (D) Stern-Volmer treatment for the dye 3/EDB fluorescence quenching; (E) Fluorescence quenching of dye 5 by Iod (speedcure 938); (F) Stern-Volmer treatment for the dye 5/Iod fluorescence quenching; (G) Fluorescence quenching of dye 5 by amine (speedcure EDB); (H) Stern-Volmer treatment for the dye 5/EDB fluorescence quenching.

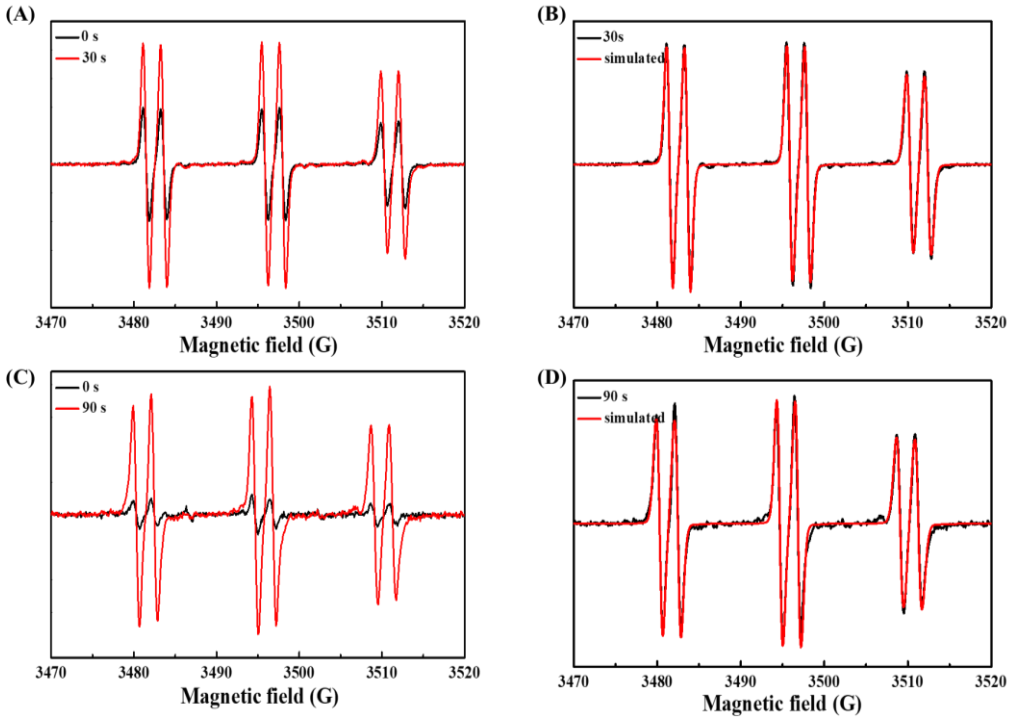

Figure S4. ESR spectra obtained from ESR-spin trapping experiment using PBN = 2 mg/mL (as spin trap agent); iodonium salt (Speedcure 938) = 12 mg/mL; amine (Speedcure EDB) = 12 mg/mL and dye 5 = 0.8 mg/mL in acetonitrile under N_2. (A) dye 5/Iod; Irradiation time = 0 s (black) and = 30 s (red) spectra; (B) dye 5/Iod; Irradiation time = 30 s (black) and simulated (red) spectra; (C) dye 5/amine; Irradiation time = 0 s (black) and = 90 s (red) spectra; (D) dye 5/amine Irradiation time = 90 s (black) and simulated (red) spectra.

Experimental part.

All reagents and solvents were purchased from Aldrich, Alfa Aesar or TCI Europe and used as received without further purification. Mass spectroscopy was performed by the Spectropole of Aix-Marseille University. ESI mass spectral analyses were recorded with a 3200 QTRAP (Applied Biosystems SCIEX) mass spectrometer. The HRMS mass spectral analysis was performed with a QStar Elite (Applied Biosystems SCIEX) mass spectrometer. Elemental analyses were recorded with a Thermo Finnigan EA 1112 elemental analysis apparatus driven by the Eager 300 software. ^{1}H and ^{13}C NMR spectra were determined at room temperature in 5 mm o.d. tubes on a Bruker Avance 400 spectrometer and on a Bruker Avance 300 spectrometer of the Spectropole: The ^{1}H chemical shifts were referenced to the solvent peak $CDCl_3$ (7.26 ppm) and the ^{13}C chemical shifts were referenced to the solvent peak $CDCl_3$ (77 ppm).

Synthesis of **2,5-*Bis*(furan-2-ylmethylene)cyclopentan-1-one**
chalcone 1

2,5-*Bis*(furan-2-ylmethylene)cyclopentan-1-one **2119**

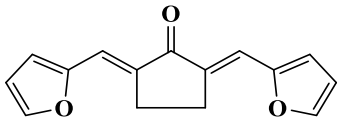

Chemical Formula: $C_{15}H_{12}O_3$
Molecular Weight: 240.2580

Yellow solid
$C_{20}H_{22}O_3$
MW = 310.39 g.mol^{-1}

Cyclopentanone (0.84 g, 10 mmol, M = 84.12 g/mol) was dissolved in a mixture of ethanol (20 mL) and water (10 mL). Furfural (1.92 g, 20 mmol, M = 96.08 g/mol) and NaOH 1M (10 mL) were then added at 0°C. The mixture was stirred at room temperature overnight. The yellow precipitate was filtrated off, washed with ethanol and dried under vacuum.

^{1}H NMR ($CDCl_3$) δ : 7.59 (d, *J* = 1.6 Hz, 1H), 7.34 (d, *J* = 7.1 Hz, 1H), 6.70 (d, *J* = 3.5 Hz, 1H), 6.54 (dd, *J* = 3.4, 1.8 Hz, 1H), 3.08 (s, 2H)

^{13}C NMR ($CDCl_3$) δ : 195.34, 152.77, 145.03, 135.89, 119.82, 115.94, 112.63, 25.80

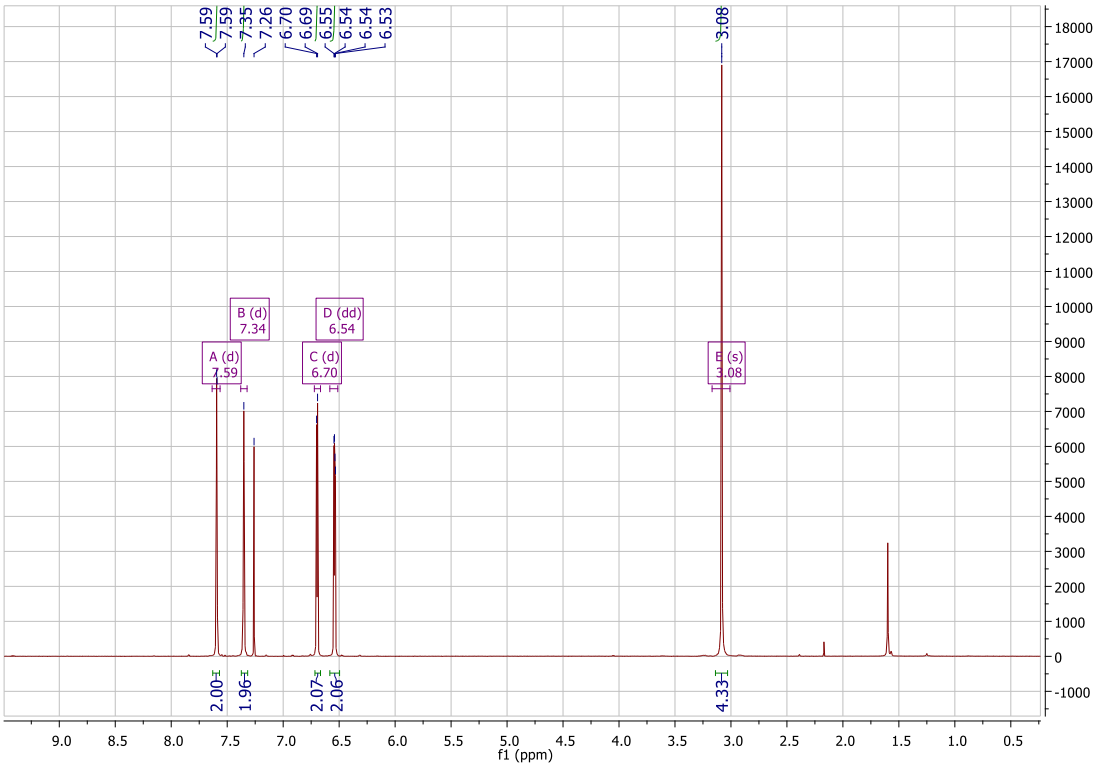

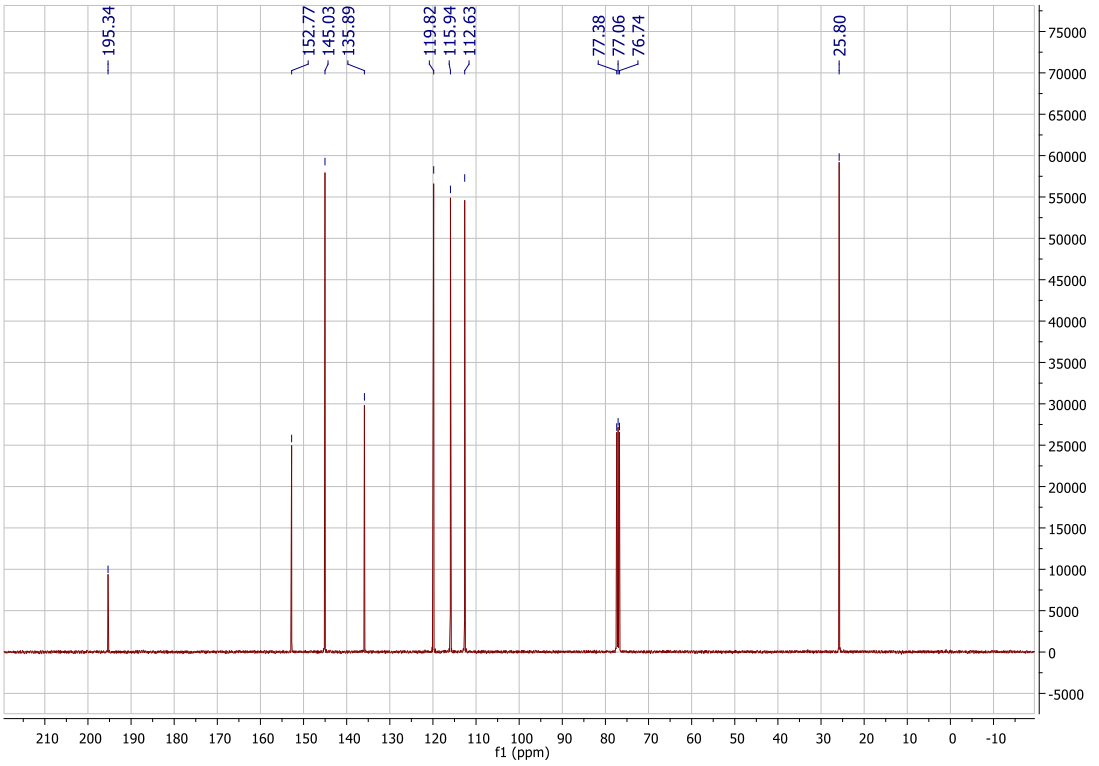

chalcone 2

2,5-*Bis*(thiophen-2-ylmethylene)cyclopentan-1-one **2118**

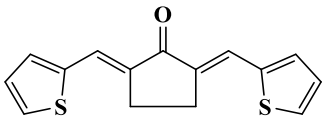

Chemical Formula: $C_{15}H_{12}OS_2$
Molecular Weight: 272.3800

Yellow solid
$C_{20}H_{22}OS_2$
MW = 342.51 g.mol^{-1}

Cyclopentanone (0.84 g, 10 mmol, M = 84.12 g/mol) was dissolved in a mixture of ethanol (20 mL) and water (10 mL). Thiophene-2-carbaldehyde (2.24 g, 20 mmol, M = 112.14 g/mol) and NaOH 1M (10 mL) were then added at 0°C. The mixture was stirred at room temperature overnight. The yellow precipitate was filtrated off, washed with ethanol and dried under vacuum.

^{1}H NMR ($CDCl_3$) δ : 7.80 (s, 2H), 7.57 (d, *J* = 5.1 Hz, 2H), 7.40 (d, *J* = 3.5 Hz, 2H), 7.17 (dd, *J* = 5.1, 3.7 Hz, 2H), 3.04 (s, 4H)

^{13}C NMR ($CDCl_3$) δ : 195.03, 140.44, 135.82, 132.63, 130.35, 128.13, 126.26, 26.05

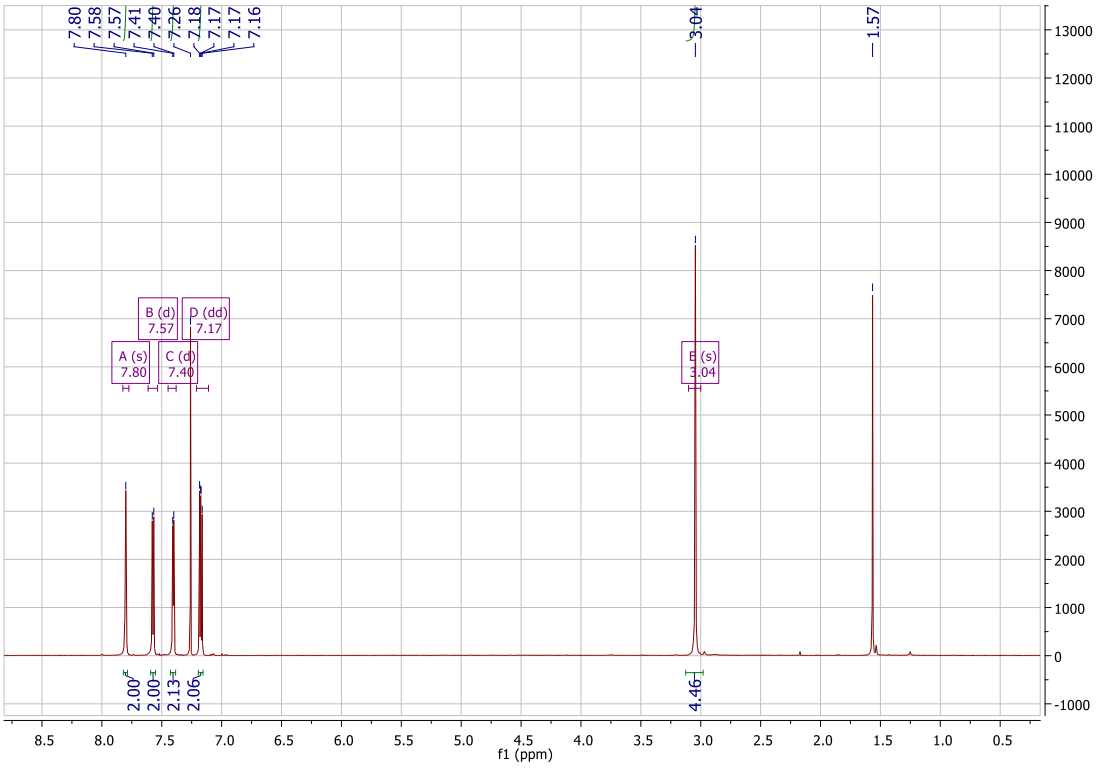

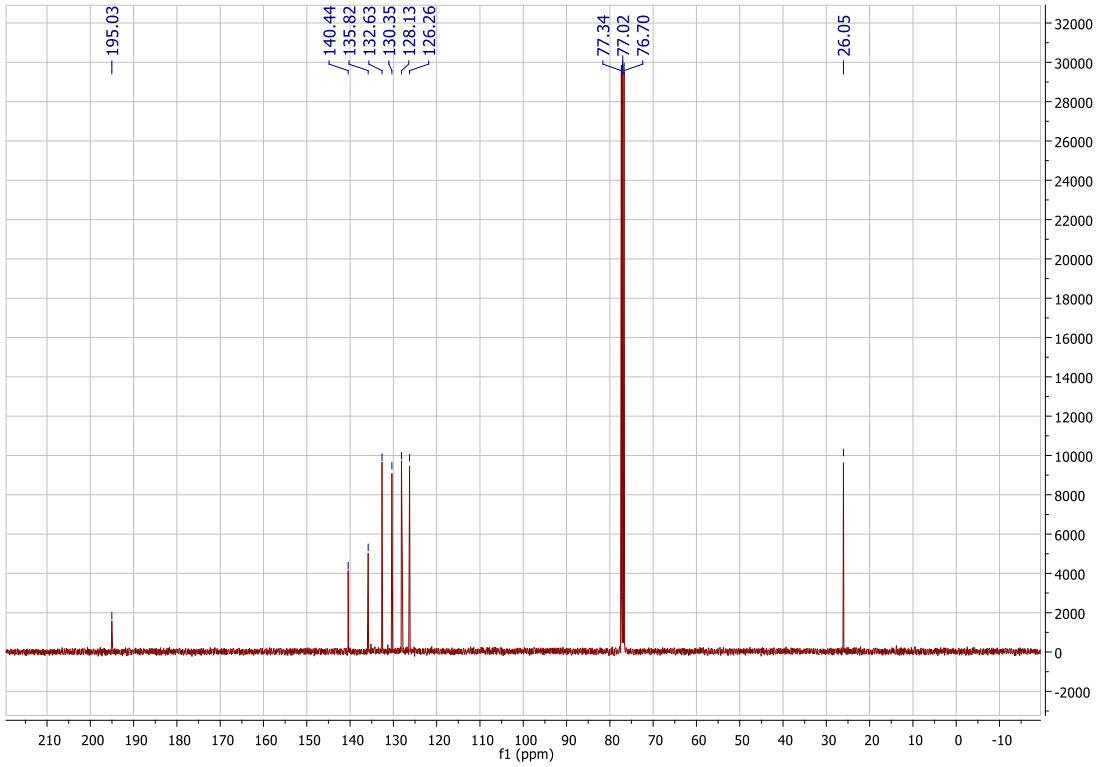

chalcone 3

2,5-*Bis*((*E*)-2,4-dibutoxybenzylidene)cyclopentan-1-one **2113**

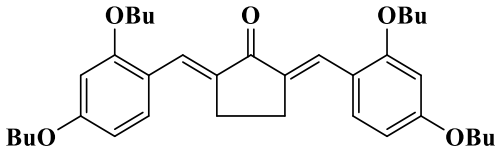

Chemical Formula: $C_{35}H_{48}O_5$
Molecular Weight: 548.7640

------ solid
$C_{24}H_{26}O_3$
MW = 362.47 g.mol^{-1}

Cyclopentanone (0.84 g, 10 mmol, M = 84.12 g/mol) was dissolved in a mixture of ethanol (20 mL) and water (10 mL). 2,4-Dibutoxybenzaldehyde (5.00 g, 20 mmol, M = 250.34 g/mol) and NaOH 1M (10 mL) were then added at 0°C. During stirring, a sticky solid formed so that THF (20-30 mL) was added to maintain the stirring of the solution. The solution was stirred at room temperature overnight. The yellow precipitate was filtrated off, washed with ethanol and dried under vacuum.

^{1}H NMR ($CDCl_3$) δ : 7.98 (s, 2H), 7.47 (d, *J* = 8.6 Hz, 2H), 6.49 (dd, *J* = 8.6, 2.3 Hz, 2H), 6.46 (d, *J* = 2.3 Hz, 2H), 3.98 (td, *J* = 6.5, 4.2 Hz, 8H), 2.96 (s, 4H), 1.87 – 1.71 (m, 8H), 1.59 – 1.42 (m, 8H), 0.98 (td, *J* = 7.4, 3.0 Hz, 12H)

^{13}C NMR ($CDCl_3$) δ : 196.10, 161.55, 160.06, 135.29, 130.82, 127.42, 118.33, 105.25,

99.52, 68.28, 67.82, 31.29, 31.22, 27.04, 19.36, 19.25, 13.88, 13.85

DFR4983

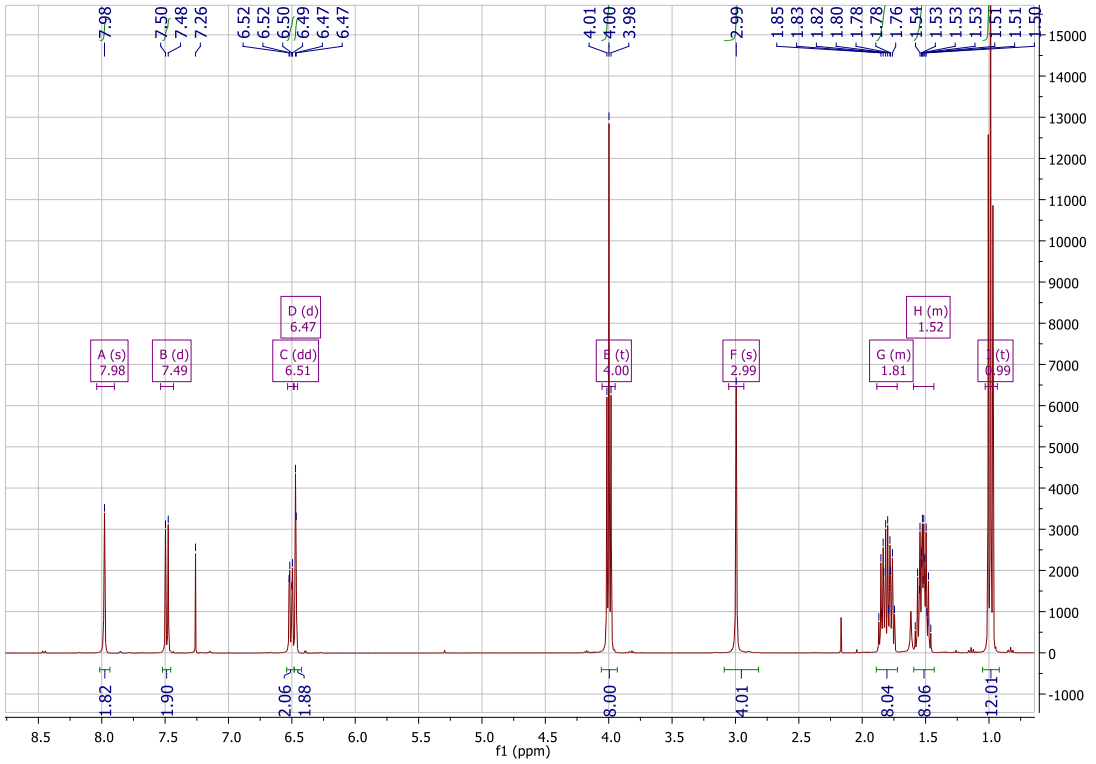

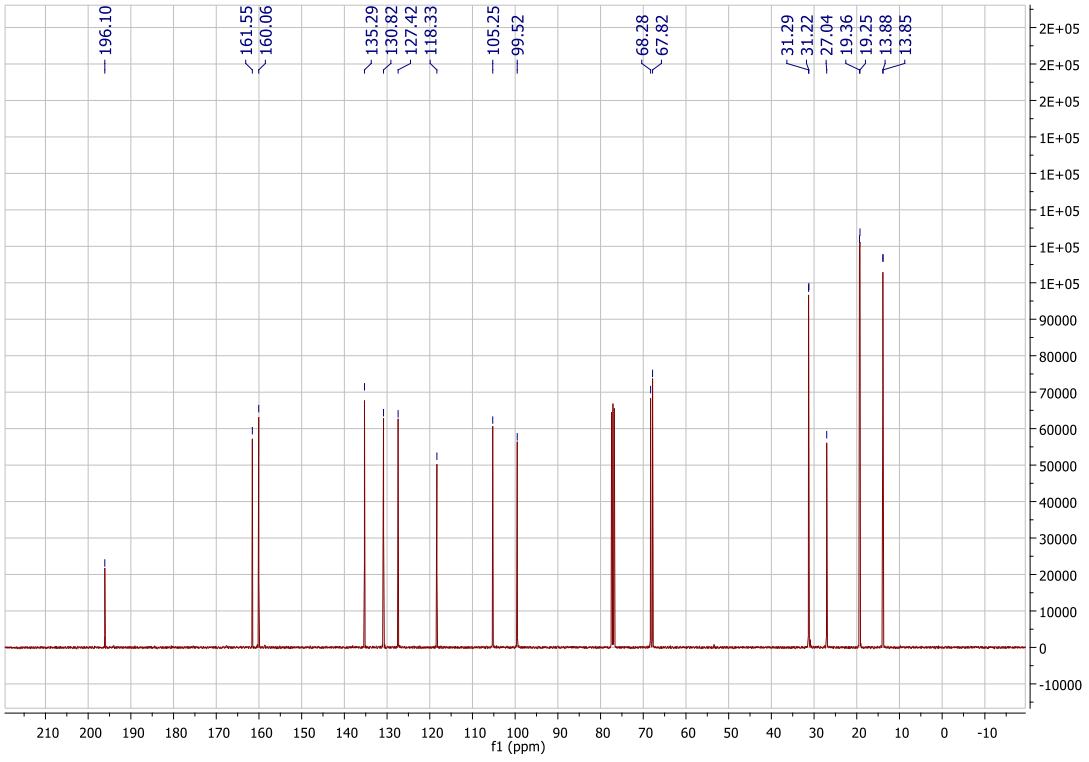

chalcone 4

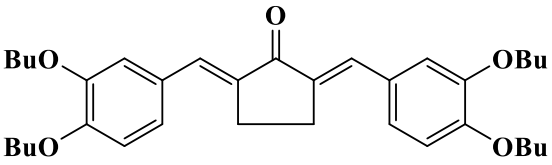

Chemical Formula: $C_{35}H_{48}O_5$
Molecular Weight: 548.7640

------ solid
$C_{24}H_{26}O_3$
MW = 362.47 g.mol^{-1}

Cyclopentanone (0.84 g, 10 mmol, M = 84.12 g/mol) was dissolved in a mixture of ethanol (20 mL) and water (10 mL). 3,4-Dibutoxybenzaldehyde (5.00 g, 20 mmol, M = 250.34 g/mol) and NaOH 1M (10 mL) were then added at 0°C. During stirring, a sticky solid formed so that THF (20-30 mL) was added to maintain the stirring of the solution. The solution was stirred at room temperature overnight. The yellow precipitate was filtrated off, washed with ethanol and dried under vacuum.

^{1}H NMR ($CDCl_3$) δ : 7.52 (s, 2H), 7.20 (dd, *J* = 8.4, 1.9 Hz, 2H), 7.15 (d, *J* = 1.9 Hz, 2H), 6.93 (d, *J* = 8.4 Hz, 2H), 4.05 (td, *J* = 6.6, 3.2 Hz, 8H), 3.10 (s, 4H), 1.83 (dt, *J* = 14.5, 6.6 Hz, 8H), 1.57 – 1.46 (m, 8H), 0.99 (td, *J* = 7.4, 3.0 Hz, 12H)

^{13}C NMR ($CDCl_3$) δ : 196.08, 150.63, 148.91, 135.26, 133.71, 128.94, 124.77, 116.23, 113.16, 69.11, 68.78, 31.31, 31.21, 26.46, 19.26, 19.22, 13.89, 13.85

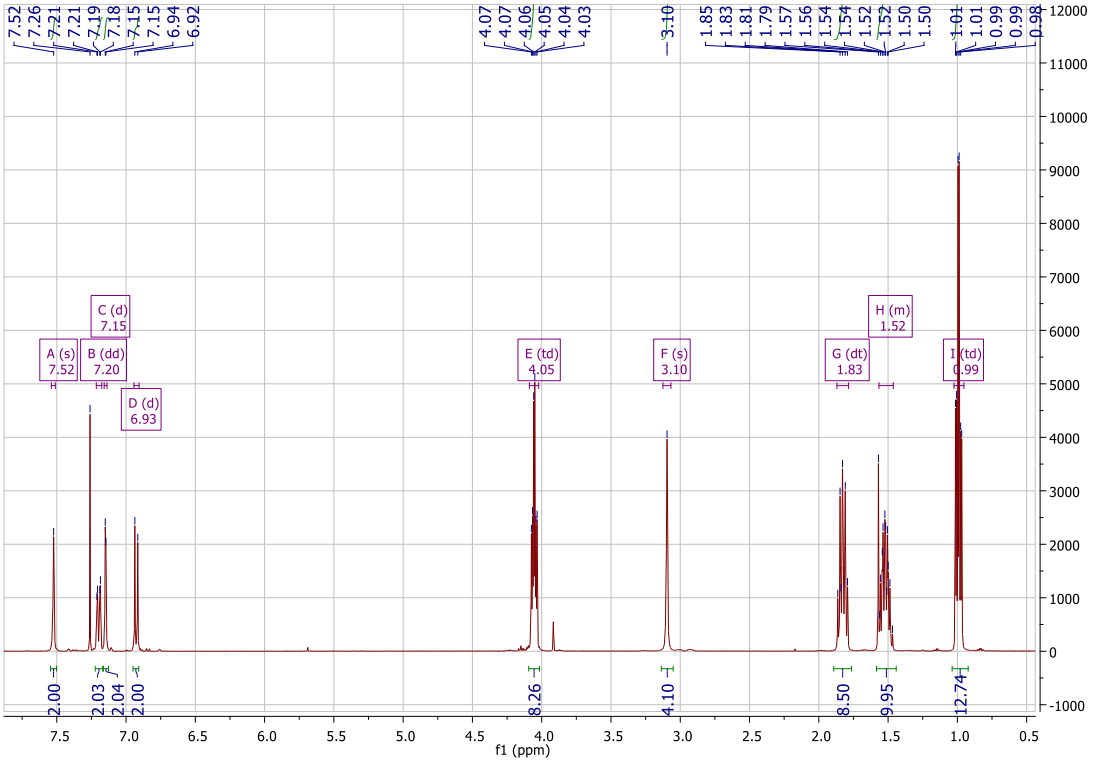

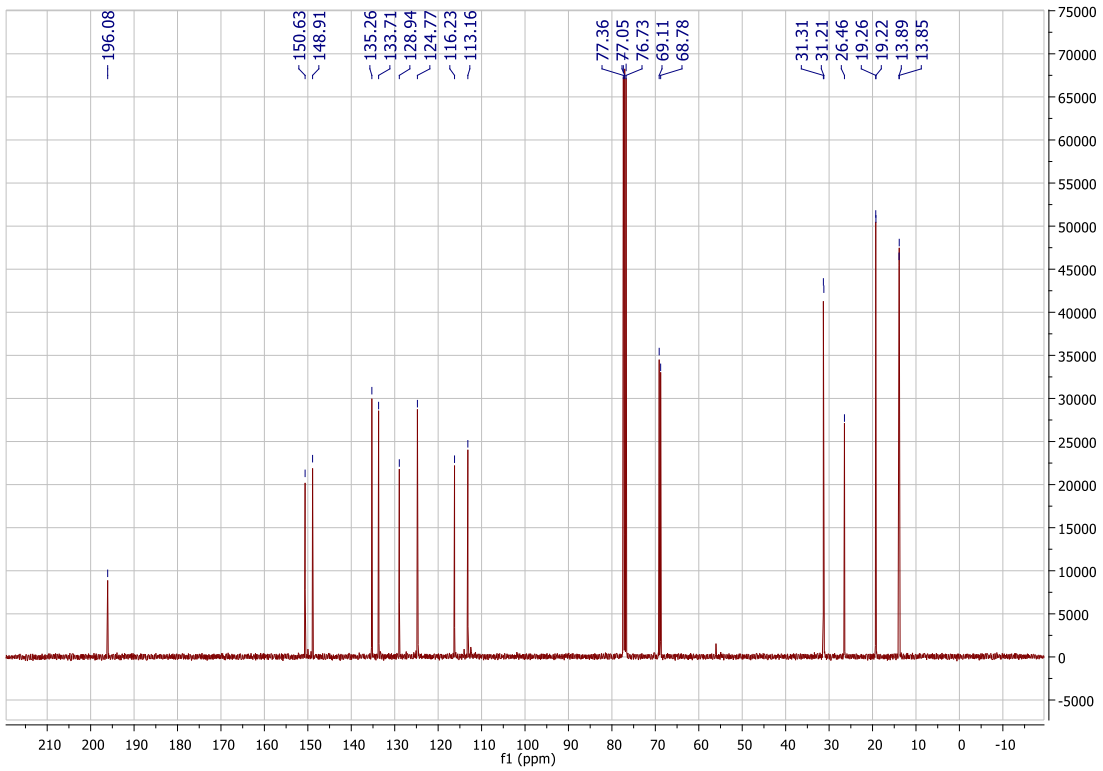

Chalcone 5: 2,5-bis((E)-4-(dimethylamino)benzylidene)cyclopentan-1-one

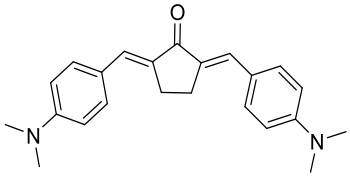

Chemical Formula: $C_{23}H_{26}N_2O$
Molecular Weight: 346,47

4-(dimethylamino)benzaldehyde (3.00 g, 20.0 mmol, M = 149.19 g/mol) and cyclopentanone (0.84 g, 10.0 mmol, M = 84.12 g/mol) were dissolved in ethanol (100 mL) and aq. KOH (40%) (15 mL) was added. The solution was stirred at room temperature overnight. During reaction, a yellow precipitate formed. It was filtered off, washed several times with ethanol and dried under vacuum.

^{1}H NMR (400 MHz, $CDCl_3$) δ 7.58 – 7.51 (m, 6H), 6.73 (d, J = 8.9 Hz, 4H), 3.07 (s, 4H), 3.04 (s, 12H).

^{13}C NMR (101 MHz, $CDCl_3$) δ 196.20, 150.86, 133.68, 132.69, 124.49, 112.08, 40.30, 26.80.

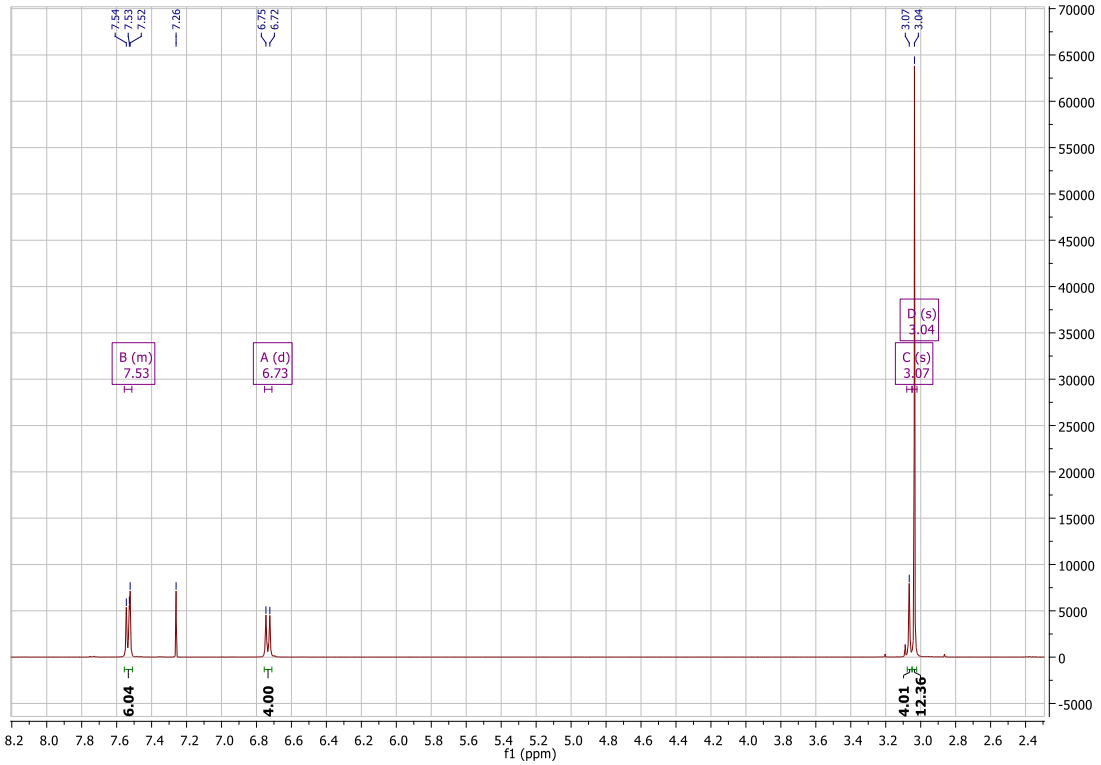

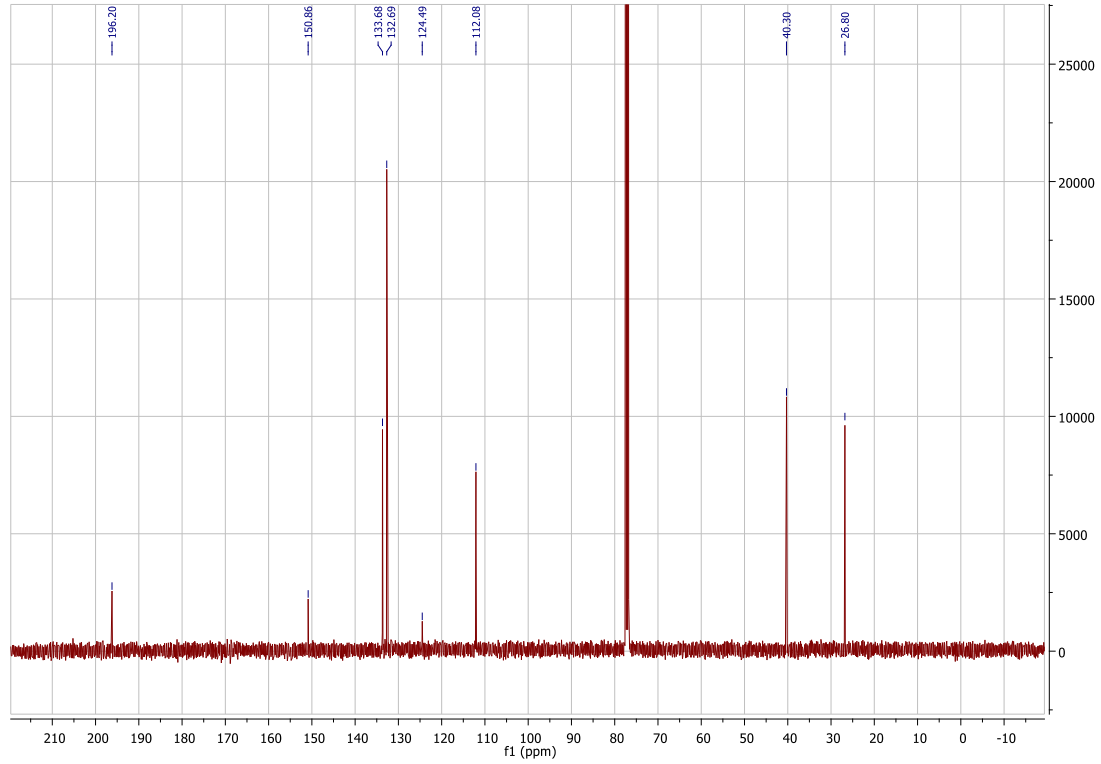

Chalcone 6: 2,5-bis((E)-2,4-bis(allyloxy)benzylidene)cyclopentan-1-one

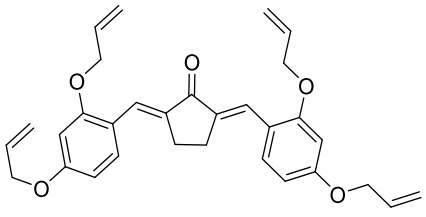

Chemical Formula: $C_{31}H_{32}O_5$
Molecular Weight: 484,59

2,4-bis(allyloxy)benzaldehyde (4.36 g, 20.0 mmol, M = 218.25 g/mol) and cyclopentanone (0.84 g, 10.0 mmol, M = 84.12 g/mol) were dissolved in ethanol (100 mL) and aq. KOH (40%) (15 mL) was added. The solution was stirred at room temperature overnight. During reaction, a yellow precipitate formed. It was filtered off, washed several times with ethanol and dried under vacuum.

^{1}H NMR (400 MHz, $CDCl_3$) δ 7.99 (s, 2H), 7.49 (d, J = 8.6 Hz, 2H), 6.54 (dd, J = 8.6, 2.3 Hz, 2H), 6.50 (d, J = 2.3 Hz, 2H), 6.15 – 5.99 (m, 4H), 5.43 (ddd, J = 17.3, 7.8, 1.4 Hz, 4H), 5.35 – 5.26 (m, 4H), 4.63 – 4.53 (m, 8H), 2.99 (s, 4H).

^{13}C NMR (101 MHz, $CDCl_3$) δ 196.22, 160.94, 159.49, 135.80, 133.00, 132.94, 130.98, 127.50, 118.88, 118.16, 117.85, 105.99, 100.34, 69.37, 69.06, 27.08.

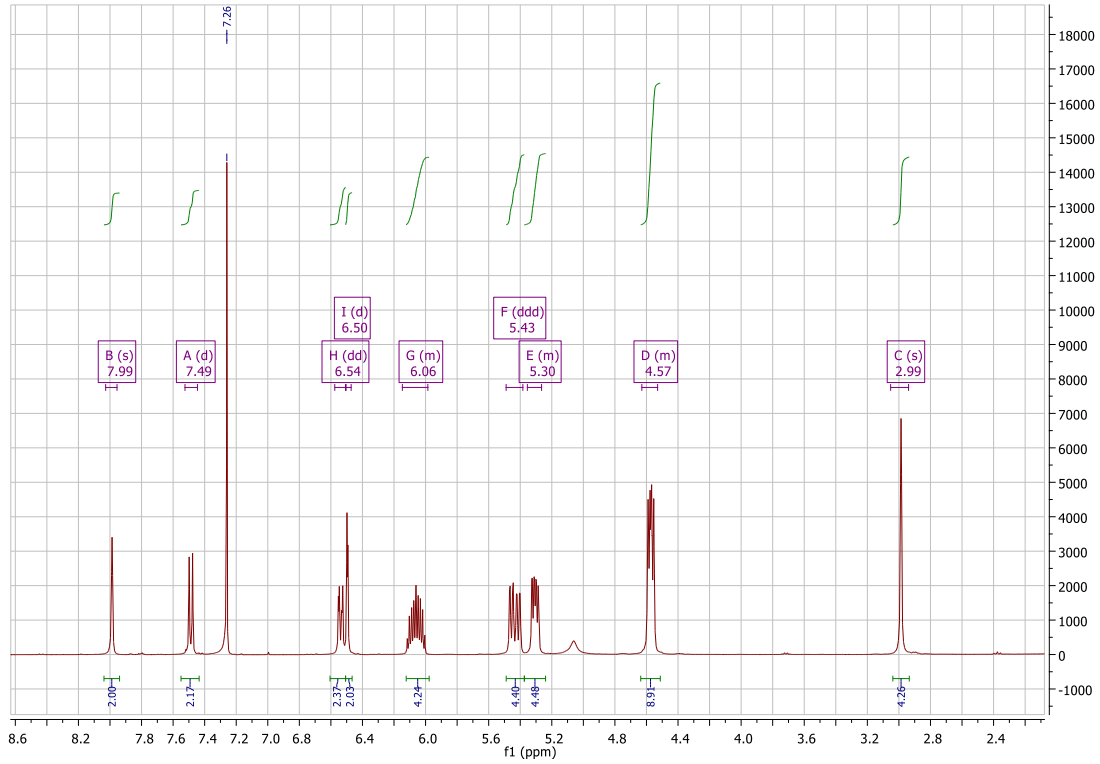

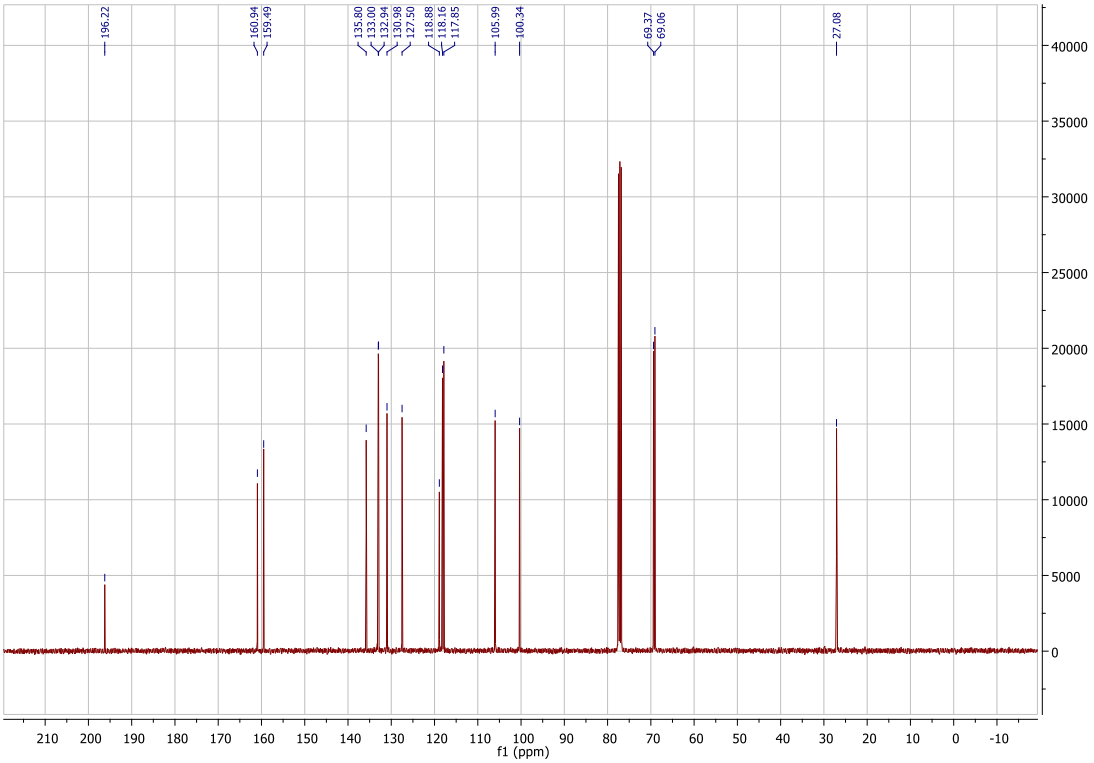

Chalcone 7: 2,5-bis((E)-2-butoxy-4-(diethylamino)benzylidene)cyclopentan-1-one

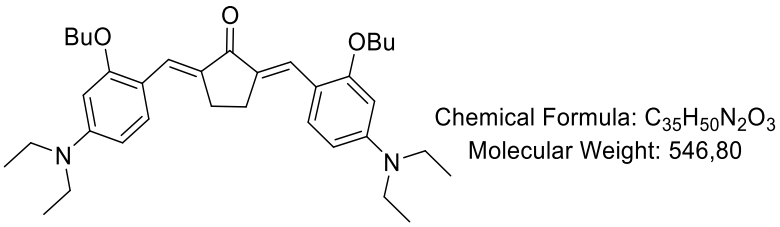

Chemical Formula: $C_{35}H_{50}N_2O_3$
Molecular Weight: 546,80

2-butoxy-4-(diethylamino)benzaldehyde (5.0 g, 20.0 mmol, M = 249.35 g/mol) and cyclopentanone (0.84 g, 10.0 mmol, M = 84.12 g/mol) were dissolved in ethanol (100 mL) and aq. KOH (40%) (15 mL) was added. The solution was stirred at room temperature overnight. During reaction, a yellow precipitate formed. It was filtered off, washed several times with ethanol and dried under vacuum.

^{1}H NMR (400 MHz, $CDCl_3$) δ 8.00 (s, 2H), 7.49 (d, J = 8.9 Hz, 2H), 6.29 (dd, J = 8.8, 2.3 Hz, 2H), 6.16 (d, J = 2.3 Hz, 2H), 4.00 (t, J = 6.4 Hz, 4H), 3.39 (q, J = 7.0 Hz, 8H), 3.00 (s, 4H), 1.89 – 1.79 (m, 4H), 1.61 – 1.50 (m, 4H), 1.20 (t, J = 7.1 Hz, 12H), 0.99 (t, J = 7.4 Hz, 6H).

^{13}C NMR (101 MHz, $CDCl_3$) δ 196.06, 160.65, 149.96, 133.20, 131.28, 127.43, 113.79, 103.93, 95.33, 68.25, 44.66, 31.49, 27.36, 19.53, 14.05, 12.87.

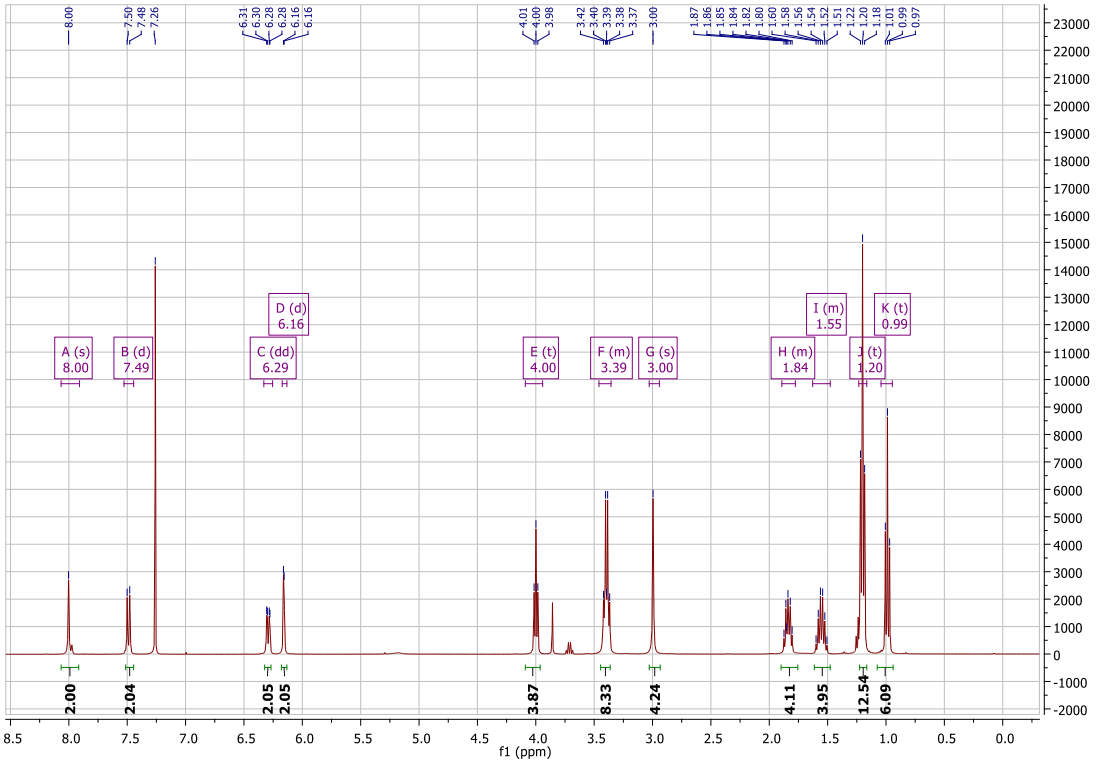

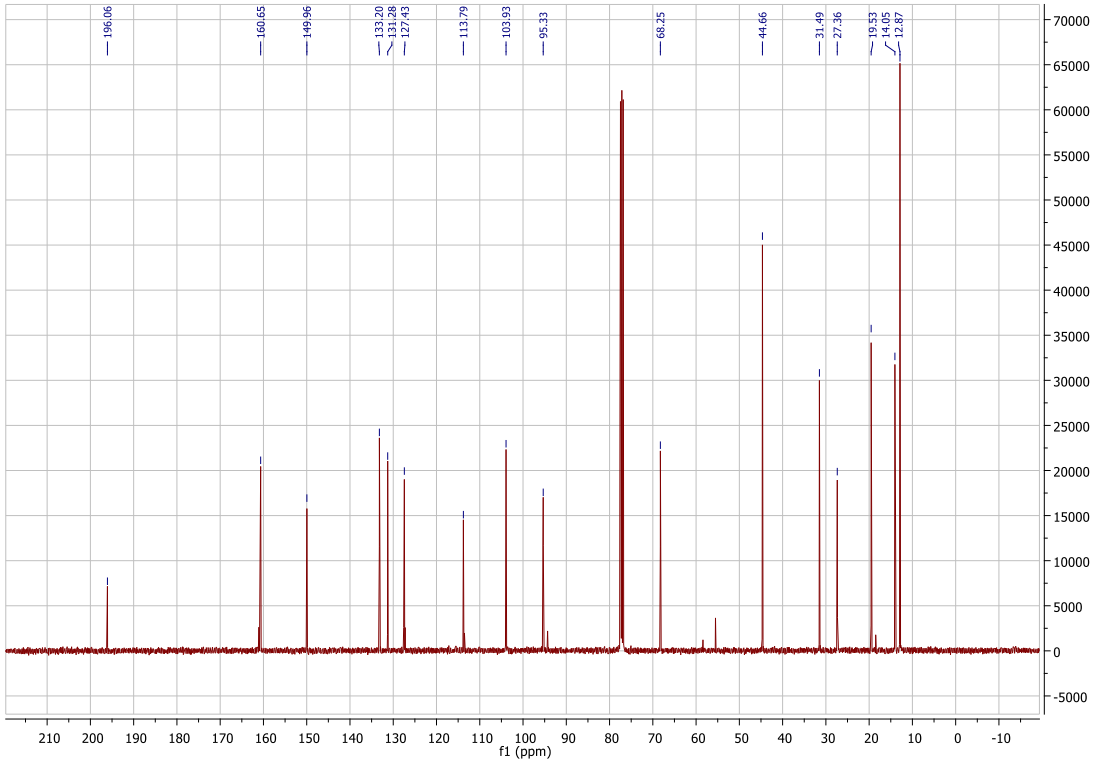

chalcone 8

2,5-*Bis*(anthracen-9-ylmethylene)cyclopentan-1-one **2120**

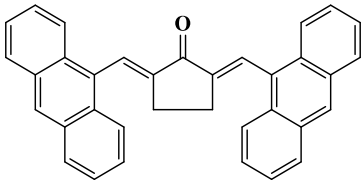

Chemical Formula: $C_{35}H_{24}O$
Molecular Weight: 460.5760

------ solid
$C_{24}H_{26}O_3$
MW = 362.47 $g.mol^{-1}$

Cyclopentanone (0.84 g, 10 mmol, M = 84.12 g/mol) was dissolved in a mixture of ethanol (20 mL) and water (10 mL). Anthracene-9-carbaldehyde (4.12 g, 20 mmol, M = 206.24 g/mol) and NaOH 1M (10 mL) were then added at 0°C. During stirring, a sticky solid formed so that THF (20-30 mL) was added to maintain the stirring of the solution. The solution was stirred at room temperature overnight. The yellow precipitate was filtrated off, washed with ethanol and dried under vacuum.

^{1}H NMR ($CDCl_3$) δ : 8.59 (s, 2H), 8.48 (s, 2H), 8.13 – 7.98 (m, 8H), 7.57 – 7.45 (m, 8H), 2.38 – 2.25 (m, 4H)

^{13}C NMR ($CDCl_3$) δ : 194.26, 144.03, 132.11, 131.27, 130.02, 129.11, 129.00, 127.92, 126.18, 125.77, 125.42, 67.98, 25.69, 25.62

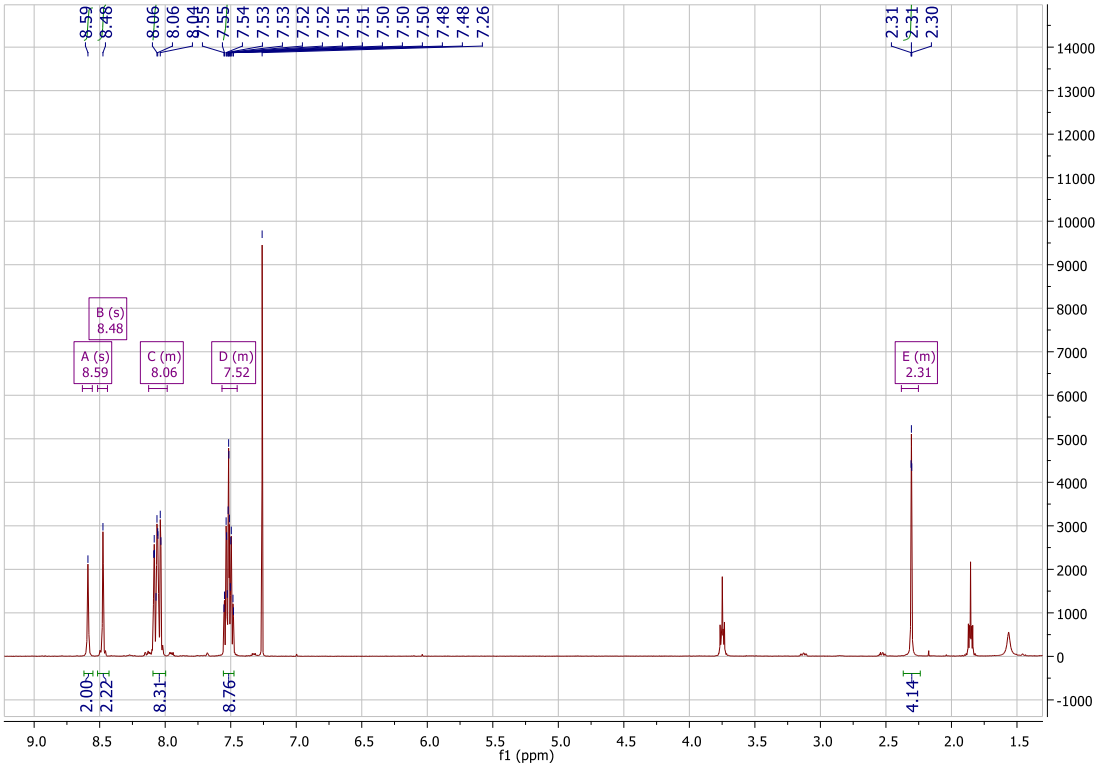

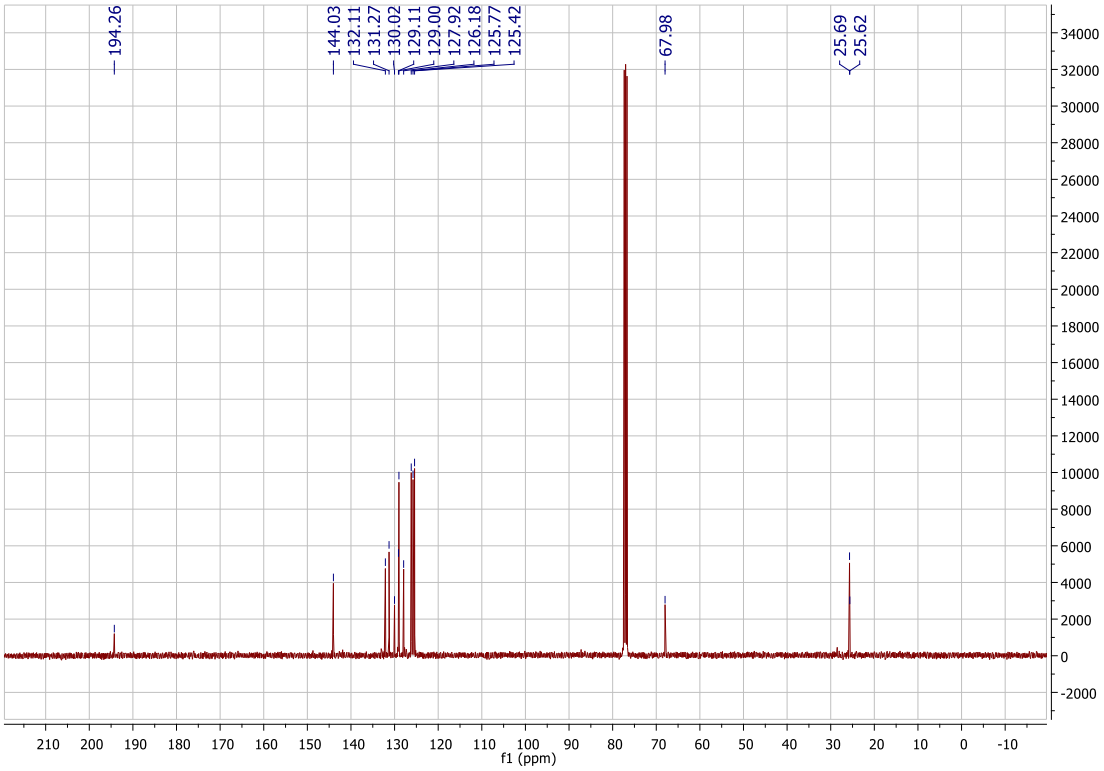

chalcone 9

2,5-*Bis*((*E*)-3-(furan-2-yl)allylidene)cyclopentan-1-one **2127**

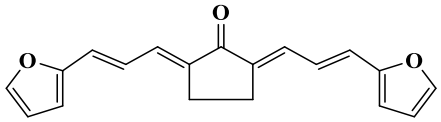

Chemical Formula: $C_{19}H_{16}O_3$
Molecular Weight: 292.3340

------ solid
$C_{24}H_{26}O_3$
MW = 362.47 g.mol^{-1}

Cyclopentanone (0.84 g, 10 mmol, M = 84.12 g/mol) was dissolved in a mixture of ethanol (20 mL) and water (10 mL). Trans-3-(2-furyl)acrolein (2.44 g, 20 mmol, M = 122.12 g/mol) and NaOH 1M (10 mL) were then added at 0°C. During stirring, a sticky solid formed so that THF (20-30 mL) was added to maintain the stirring of the solution. The solution was stirred at room temperature overnight. The yellow precipitate was filtrated off, washed with ethanol and dried under vacuum.

^{1}H NMR ($CDCl_3$) δ : 7.45 (d, *J* = 1.4 Hz, 2H), 7.17 (d, *J* = 11.7 Hz, 2H), 6.85 (dd, *J* = 15.3, 11.7 Hz, 2H), 6.72 (d, *J* = 15.3 Hz, 2H), 6.50 – 6.41 (m, 4H), 2.88 (s, 4H)

^{13}C NMR ($CDCl_3$) δ : 194.66, 152.86, 143.70, 140.15, 132.19, 127.39, 123.28, 112.32, 111.98, 23.92

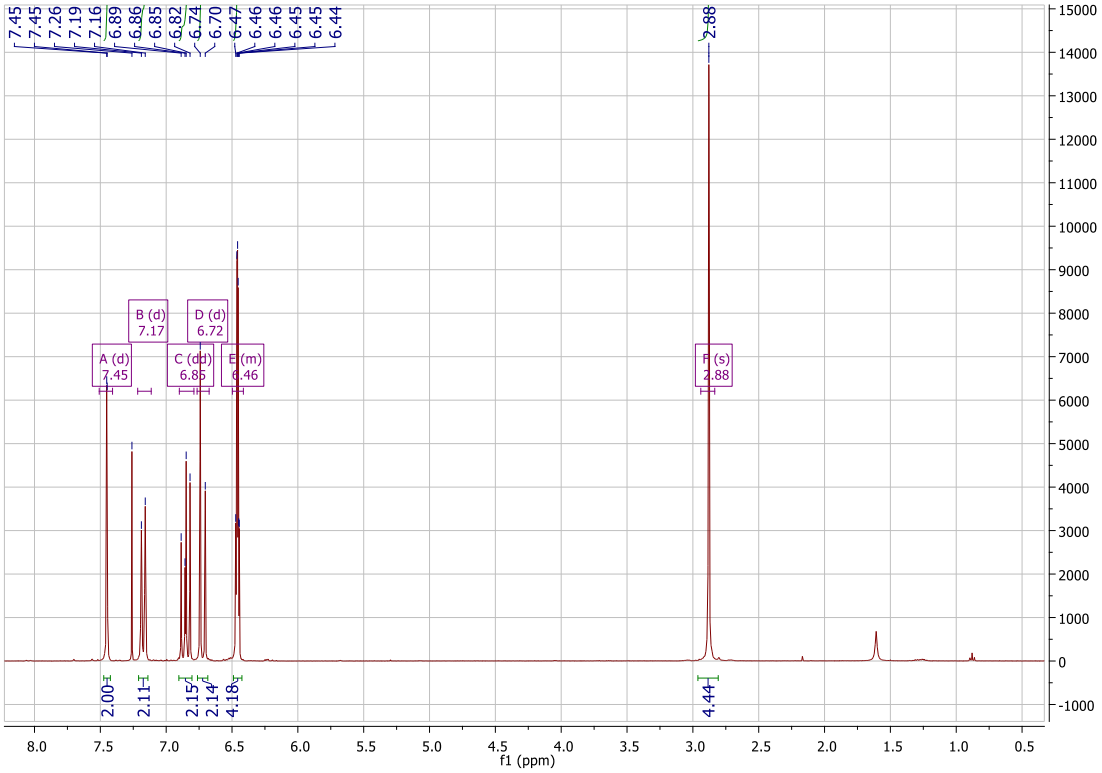

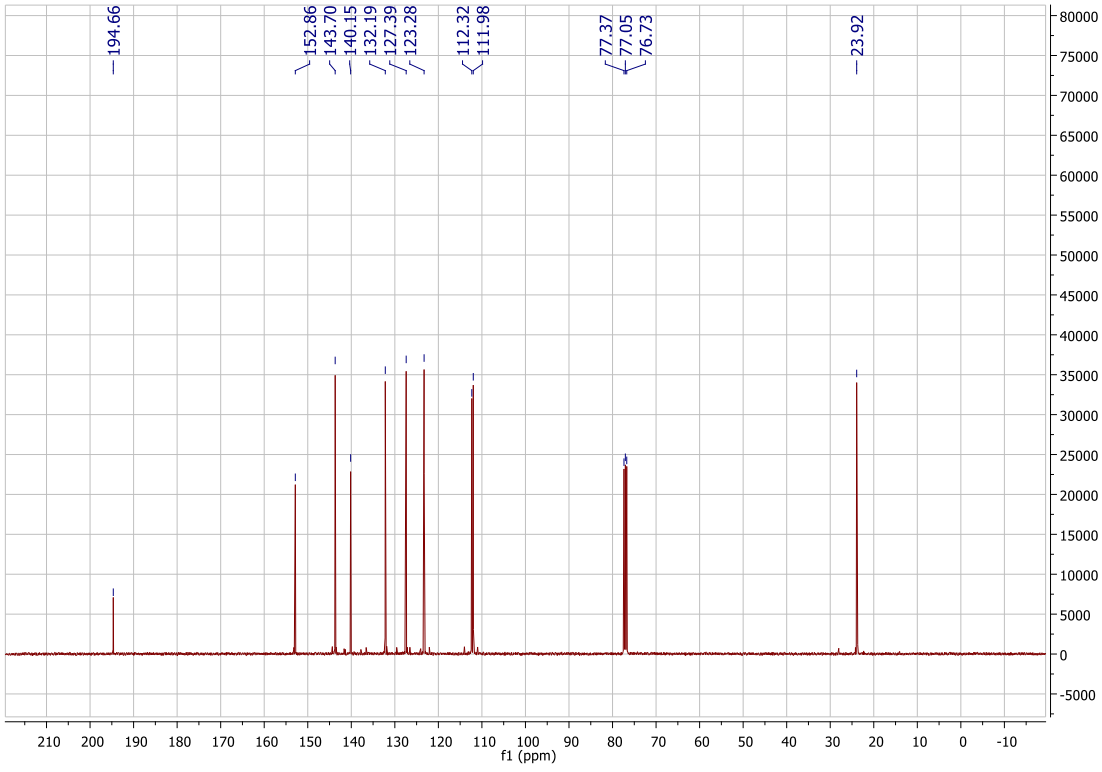

chalcone 10

2,5-*Bis*((*E*)-2,4,5-trimethoxybenzylidene)cyclopentan-1-one **2131**

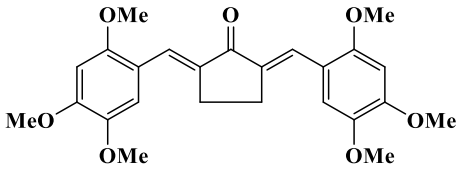

Chemical Formula: $C_{25}H_{28}O_7$
Molecular Weight: 440.4920

------ solid
$C_{24}H_{26}O_3$
MW = 362.47 g.mol^{-1}

Cyclopentanone (0.84 g, 10 mmol, M = 84.12 g/mol) was dissolved in a mixture of ethanol (20 mL) and water (10 mL). 2,4,5-Trimethoxybenzaldehyde (3.92 g, 20 mmol, M = 196.20 g/mol) and NaOH 1M (10 mL) were then added at 0°C. During stirring, a sticky solid formed so that THF (20-30 mL) was added to maintain the stirring of the solution. The solution was stirred at room temperature overnight. The yellow precipitate was filtrated off, washed with ethanol and dried under vacuum.

^{1}H NMR ($CDCl_3$) δ : 7.96 (s, 2H), 7.11 (d, *J* = 14.8 Hz, 2H), 6.53 (s, 2H), 3.99 – 3.91 (m, 6H), 3.87 (d, *J* = 7.1 Hz, 12H), 3.06 (s, 4H)

^{13}C NMR ($CDCl_3$) δ : 195.87, 154.90, 151.37, 142.73, 135.18, 127.57, 116.94, 113.10, 96.89, 56.60, 56.48, 56.02, 26.81

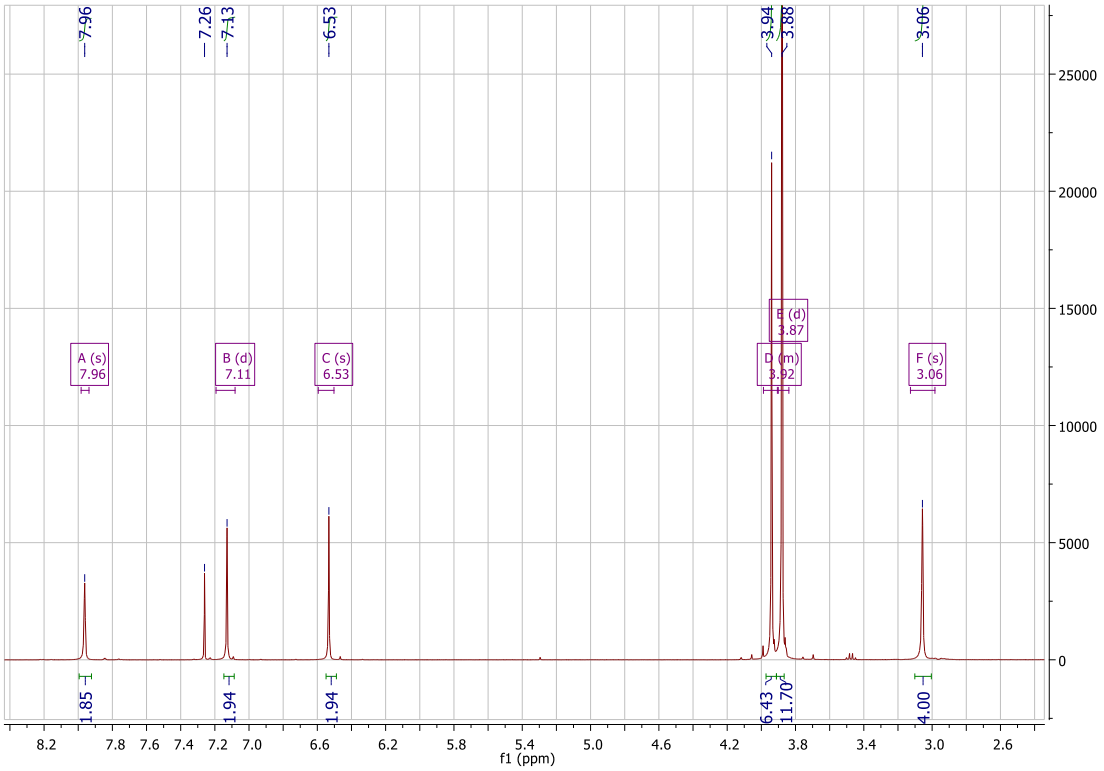

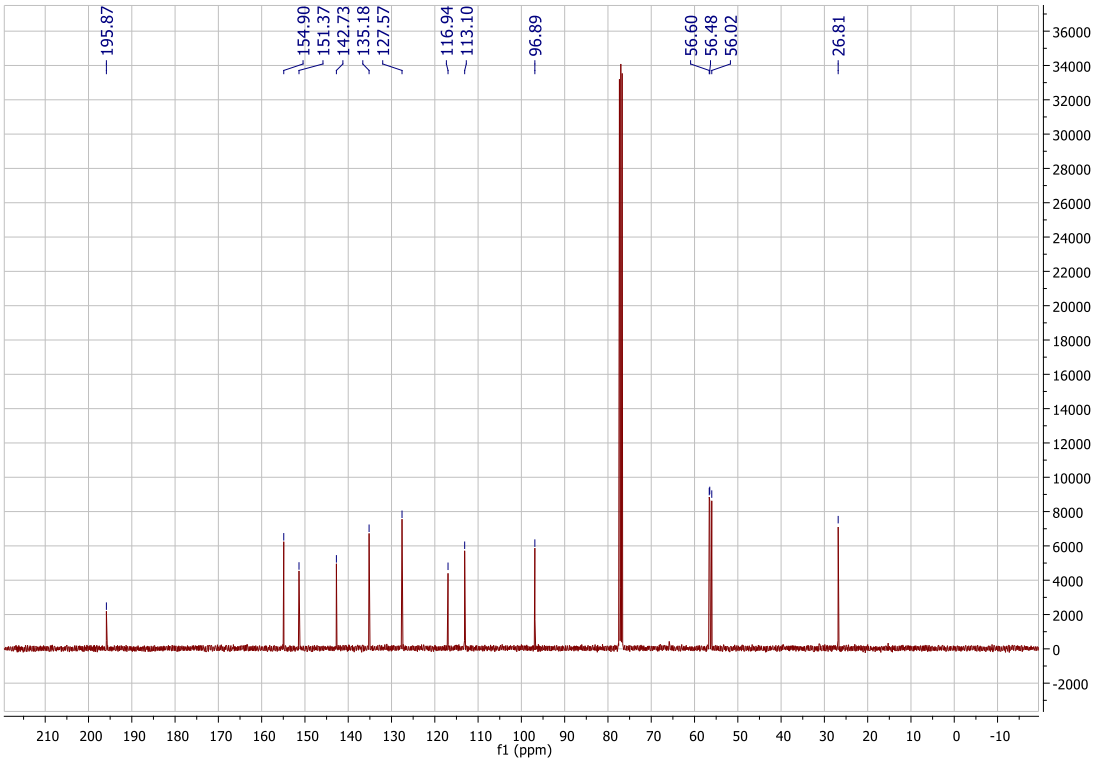

chalcone 11

2,5-*Bis*((9-benzyl-9*H*-carbazol-3-yl)methylene)cyclopentan-1-one **2139**

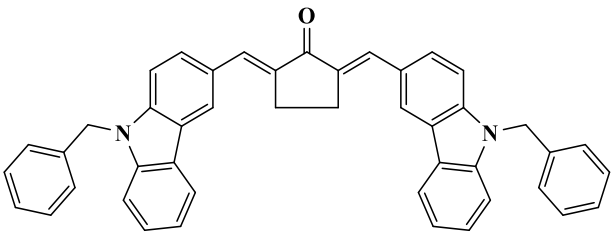

Chemical Formula: $C_{45}H_{34}N_2O$
Molecular Weight: 618.7800

------ solid
$C_{24}H_{26}O_3$
MW = 362.47 g.mol^{-1}

Cyclopentanone (0.84 g, 10 mmol, M = 84.12 g/mol) and 9-benzyl-9*H*-carbazole-3-carbaldehyde (5.71 g, 20 mmol, M = 285.35 g/mol) was dissolved in ethanol (50 mL) and KOH (40%) was added. THF was added until complete dissolution of carbazole was obtained. The solution was stirred at room temperature for 48h. During that time, a precipitate formed. It was filtered off, washed with water, ether and dried under vacuum.

^{1}H NMR ($CDCl_3$) δ : 8.39 (s, 2H), 8.18 (d, *J* = 7.6 Hz, 2H), 7.85 (s, 2H), 7.72 (dd, *J* = 8.6, 1.4 Hz, 2H), 7.49 – 7.44 (m, 2H), 7.39 (dd, *J* = 13.8, 5.9 Hz, 4H), 7.30 (ddd, *J* = 8.6, 7.7, 2.1 Hz, 8H), 7.17 – 7.12 (m, 4H), 5.53 (s, 4H), 3.26 (s, 4H)

^{13}C NMR ($CDCl_3$) δ : trop insoluble

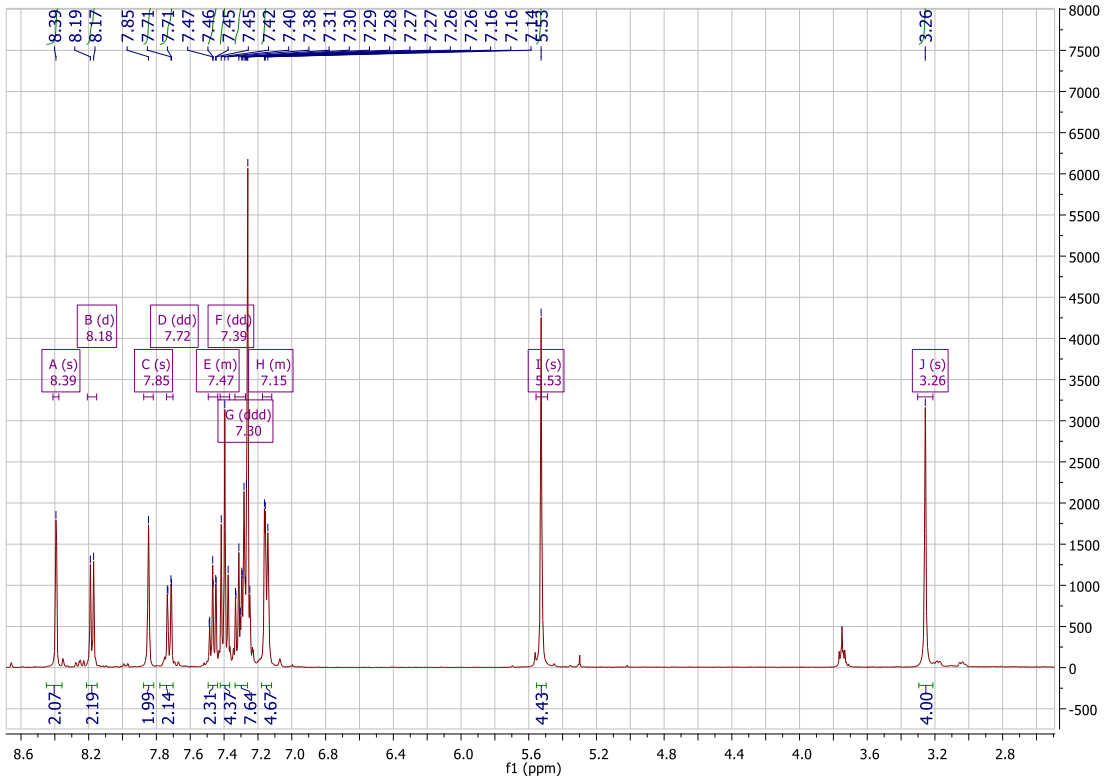

Chalcone 12: 2,5-bis((E)-4-(diphenylamino)benzylidene)cyclopentan-1-one

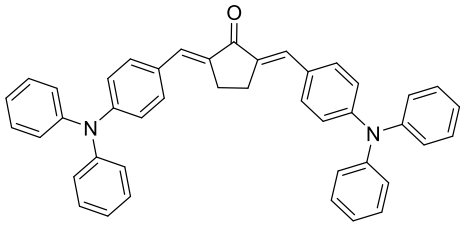

Chemical Formula: $C_{43}H_{34}N_2O$
Molecular Weight: 594,76

4-(diphenylamino)benzaldehyde (5.46 g, 20.0 mmol, M = 273.34 g/mol) and cyclopentanone (0.84 g, 10.0 mmol, M = 84.12 g/mol) were dissolved in ethanol (100 mL) and aq. KOH (40%) (15 mL) was added. The solution was stirred at room temperature overnight. During reaction, a yellow precipitate formed. It was filtered off, washed several times with ethanol and dried under vacuum.

^1H NMR (300 MHz, $CDCl_3$) δ 7.53 (s, 2H), 7.46 (d, J = 8.8 Hz, 4H), 7.33 – 7.27 (m, 8H), 7.17 – 7.12 (m, 10H), 7.08 – 7.02 (m, 6H), 3.06 (s, 4H).

^{13}C NMR (101 MHz, $CDCl_3$) δ 196.17, 148.99, 147.02, 135.46, 133.26, 132.12, 129.85, 129.60, 129.30, 126.43, 125.54, 125.48, 124.13, 121.69, 26.71.

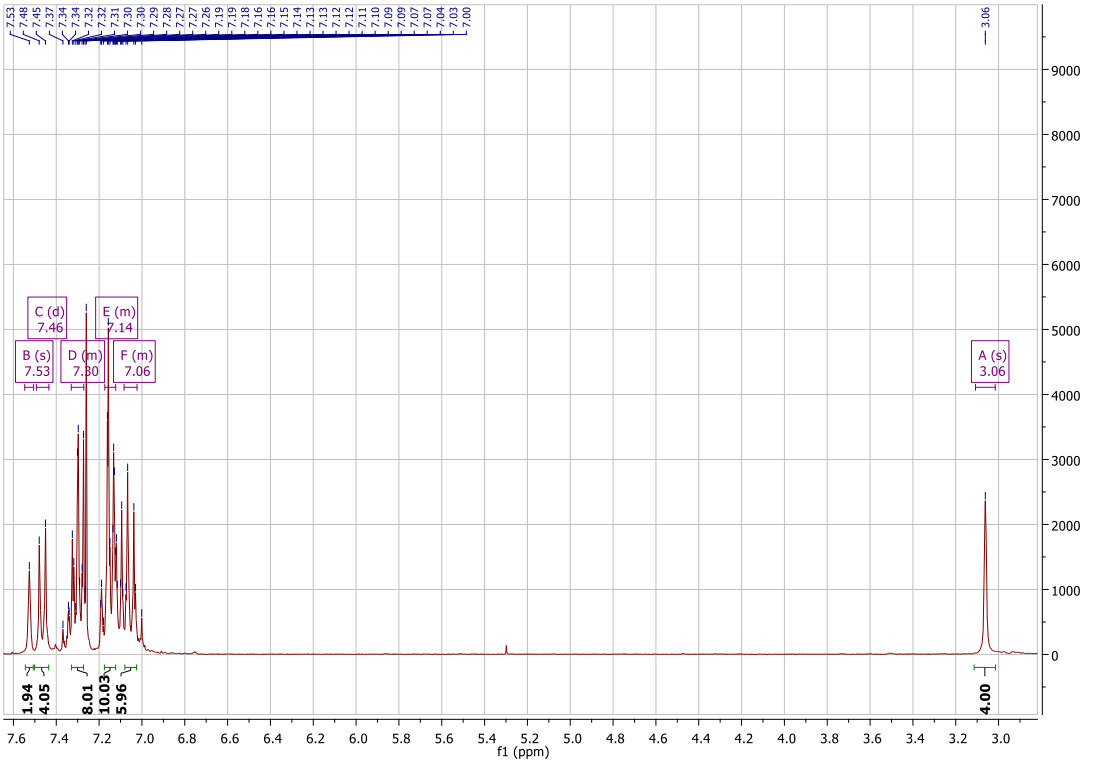
C (d)
7.46
E (m)
7.14
B (s)
7.53
D (m)
7.30
F (m)
7.06
A (s)
3.06
1.94
4.05
8.01
10.03
5.96
4.00
f1 (ppm)

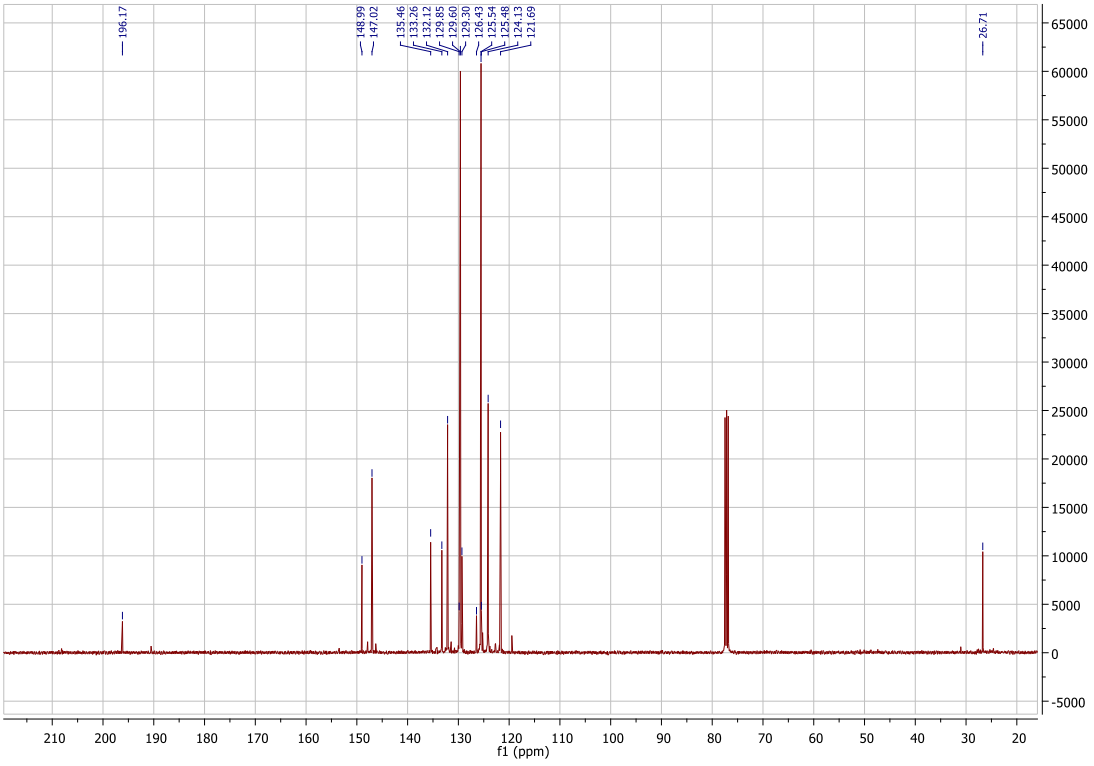
196.17
148.99
147.02
135.46
133.26
132.12
129.85
129.60
129.30
126.43
125.54
125.48
124.13
121.69
26.71
f1 (ppm)